NASA Contractor Report 182014

MILLIMETER WAVE NEAR-FIELD STUDY

Neill Kefauver

Near-Field Test Laboratory
Martin Marietta Astronautics Group
Denver, Colorado

Contract NAS1-18455
April 1990

National Aeronautics and
Space Administration

Langley Research Center
Hampton, Virginia 23665-5225

TABLE OF CONTENTS

LIST OF TABLES

LIST OF FIGURES

1.0 INTRODUCTION

The purpose of the Millimeter Wave Near-Field Study Task, performed under contract NAS1-18455 by the Near-Field Measurement Laboratory (NFML) of the Martin Marietta Astronautics Group, Space Systems Company, was to quantify the system upgrade requirements necessary to accomplish successful measurements of large spacecraft antennas operating at millimeter wavelengths. Several initial assumptions were made about the future test article prior to performing this task. These assumptions include the following:

Maximum facility lifting capacity is one ton

Aperture is less than 15 meters in diameter

Unit center of gravity will be centered on the NFML rotary table

Antenna directivity will exceed 30 dB

Millimeter power needs will not exceed commercial supplies

Planar near-field will be the scan geometry

NFML will provide the calibration of standards

Measurements will use harmonic mixing

Collection array sizes will not exceed 2048 by 2048 points

The results of this task include a prediction of measurement errors for the facility upgrade, a cost analysis of the software and hardware required for this upgrade, and a summary of the diagnostics available to improve the performance of the unit while it is being measured in the NFML. Technical concerns addressed in the task report consist of scanner positioning, system accuracy, cabling stability, measurement time, processing time, dynamic range of the measurements and millimeter measurement hardware requirements.

The task report is divided into seven sections: introduction, theoretical error modeling, experimental verification, error predictions, diagnostics, cost summary, and conclusions. The error model predicts the contribution to measurement accuracy of arbitrary but known error sources: position error, system drift, system linearity, and system noise. The experimental verification will use measurements of existing laboratory hardware to determine the validity of model predictions. The section on error predictions will combine theory and experiment to define the potential performance of the NFML after the millimeter upgrade. The diagnostic section will briefly cover the capabilities of the NFML to use knowledge of the physical structure of the antenna with near-field measurements to determine sources of antenna degradation and possible methods of improving the antenna performance. The section summarizing the cost of facility upgrades will detail the cost expectation of upgrades to several frequency bands, the estimates will be given in manhours and material dollars. The estimates are only technical and shall not be used for contract pricing. The conclusions section will summarize the optimum approach to prepare the facility for the customer measurement requirements.

2.0 Error Model Derivation

To accurately propose a near-field scanner for performing millimeter wavelength measurements, a model was required to relate far-field pattern errors to near-field measurement system errors. This model determines pattern measurement errors arising from scanner mispositioning, system drift, and system noise. Several other error sources were added to the model after experimental measurement. These sources include cable flexure, measurement repeatability, and system linearity. The resulting model allows the prediction of NFML measurement accuracies and limitations through the millimeter band based upon known performance at frequencies below 18 GHz.

Sections 2.1 through 2.4 will detail the aspects of the theoretical model development. In section 2.1 the general position error model is developed. This model predicts the errors resulting from mispositioning. Section 2.2 covers how a systematic long-term drift (over several hours) can be compensated. Section 2.3 specifically addresses the errors introduced by the specialized scanning modes of the NFML, quadrant and bifurcated. Section 2.4 discusses how short term drift can affect the final measurement results. Sections 3.0 to 3.5 explain the methods used to convert the experimental data into additional modeling capability in the millimeter scanner model.

2.1 Position Errors

Pattern measurement inaccuracies caused by position errors (relative to a perfect planar grid) can easily be modeled using Taylor series expansions about the grid points. In the NFML these errors arise from several sources: misadjustment of the scanner ways, scanner positioning repeatability, probe misalignment, and turntable tilt. Mathematical relationships had to be determined that would describe the behavior of the positioning error sources. Measured positioning data yielded approximate values for each error source in the model. The following table lists the assumed root mean square average of each source modeled.

Table 1: Positioning Error Components and Their Magnitude

Component	Magnitude	
	English	Metric
Y-Axis Mechanical Alignment (in z)	0.008"	200 mm
Y-Axis Positioning Repeatability (in z)	0.001"	25 mm
X-Axis Mechanical Alignment (in z)	0.001"	25 mm
X-Axis Positioning Repeatability (in z)	0.0002"	5 mm
Turntable Tilt, θ_t*	0.006°	100 μradians**
Turntable Pitch, θ_p	0.003°	50 μradians**
Turntable Roll, θ_r	0.003°	50 μradians**

*Turntable tilt contributes to z position error in the NFML when the aperture is too large for rectangular scans. The tilt corresponds to the rotational non-perpendicularity of the turntable to gravity

**For an understanding of the NFML use of these terms, see Figure 1. For comparison to scan axes straightness data, consider that, if a 5 meter radial aperture is tilted 0.001° (17.5 μradians), the aperture edge will be displaced 0.0034" (87.5 microns).

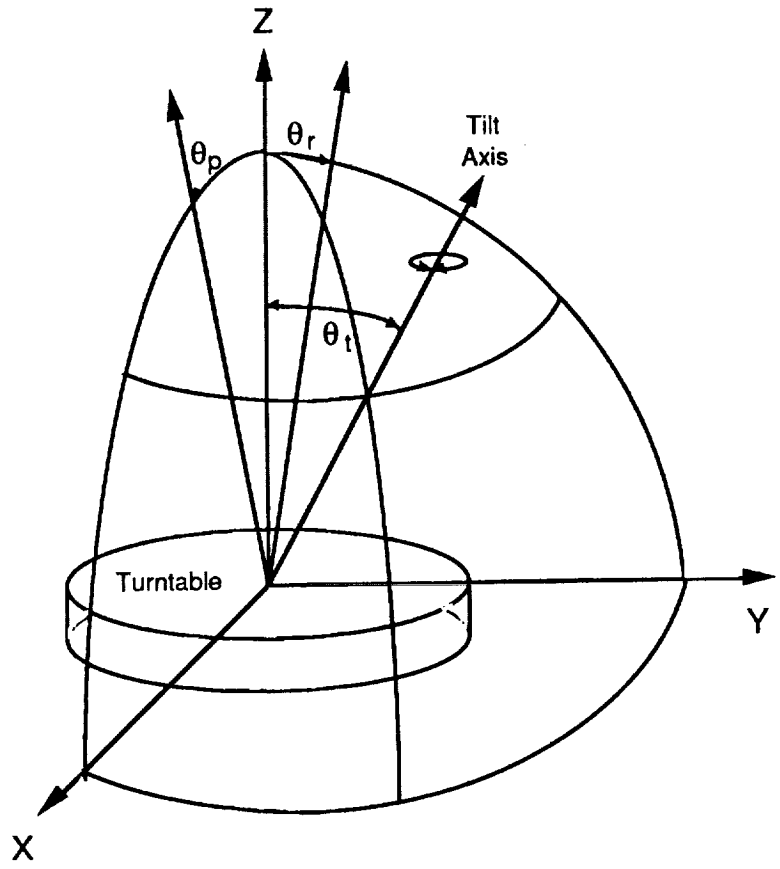

Figure 1 Misalignment Angles of the NFML Turntable

As the Table 1 clearly shows the largest components of position error are the Y-Axis mechanical alignment and the three components of turntable non-planarity for large aperture antennas. Clearly, the resulting near-field measurement errors from these components must be understood completely if millimeter measurements at the NFML are to be successful. The initial analysis neglected contributions of transverse mispositioning, primarily because the antenna pattern was assumed to be highly directive resulting in a small tangential derivative. The assumption of high directivity is valid for any millimeter antenna with an aperture size exceeding a foot (30 wavelengths). In Cartesian coordinates as shown in Figure 1, the general relationship between a field at a perturbed position and the field at the correct position is expressed by equation 1, which is a Taylor series expansion in three dimensions.[1]

$$\bar{E}_c=\sum_{i=0}^{\infty}\sum_{j=0}^{\infty}\sum_{k=0}^{\infty}\frac{\delta_x^j\delta_y^i\delta_z^k}{i!\ j!\ k!}\left(\frac{\partial^i}{\partial x^i}\left(\frac{\partial^j}{\partial y^j}\left(\frac{\partial^k}{\partial z^k}(\bar{E}_m)\right)\right)\right) \tag{1}$$

$\bar{E}_c = \bar{E}_c(x_c,y_c,z_c)$ = the electric field at the correct grid position

$\bar{E}_m= \bar{E}_m(x_m,y_m,z_m)$= the electric field at the measurement point

$(x_c,y_c,z_c) = \bar{r}$ = correct grid point

$(x_m,y_m,z_m)=(x_c+\delta_x, y_c+\delta_y, z_c+\delta_z)=\bar{r} + \bar{\delta}$ = the measurement point

$\frac{\partial^i}{\partial x^i}, \frac{\partial^j}{\partial y^j}, \frac{\partial^k}{\partial z^k}$ are ith, jth, and kth order partial derivatives of the electric field of x,y, and z

i!,j!,and k! are the factorials of i,j, and k respectively

If the derivatives in x and y are neglected then equation 1 can be asymptotically approximated by equation 2, this approximation should be true for large aperture antenna.

$$\bar{E}_c=\sum_{k=0}^{\infty}\frac{\delta_z^k}{k!}\left(\frac{\partial^k}{\partial z^k}(\bar{E}_m)\right) \tag{2}$$

To determine if this simplification is valid for the predicted positioning errors, a typical measured antenna pattern was modified by a file of errors asymptotic to equation 1 and also a set satisfying equation 2. Figure 2 shows a far-field principal plane overlay of the error free file with results from equation 1 and the residue difference between the results from equations 1 and 2. Assumed antenna gain was 65 dB at 60 GHz and the aperture was scanned in bifurcated mode. Partial derivatives are determined using a special behavior of the Fourier transform, which is is also used to determine the far-field pattern from the near-field data. Equation 3 shows the fundamental relationship used in this application.[2]

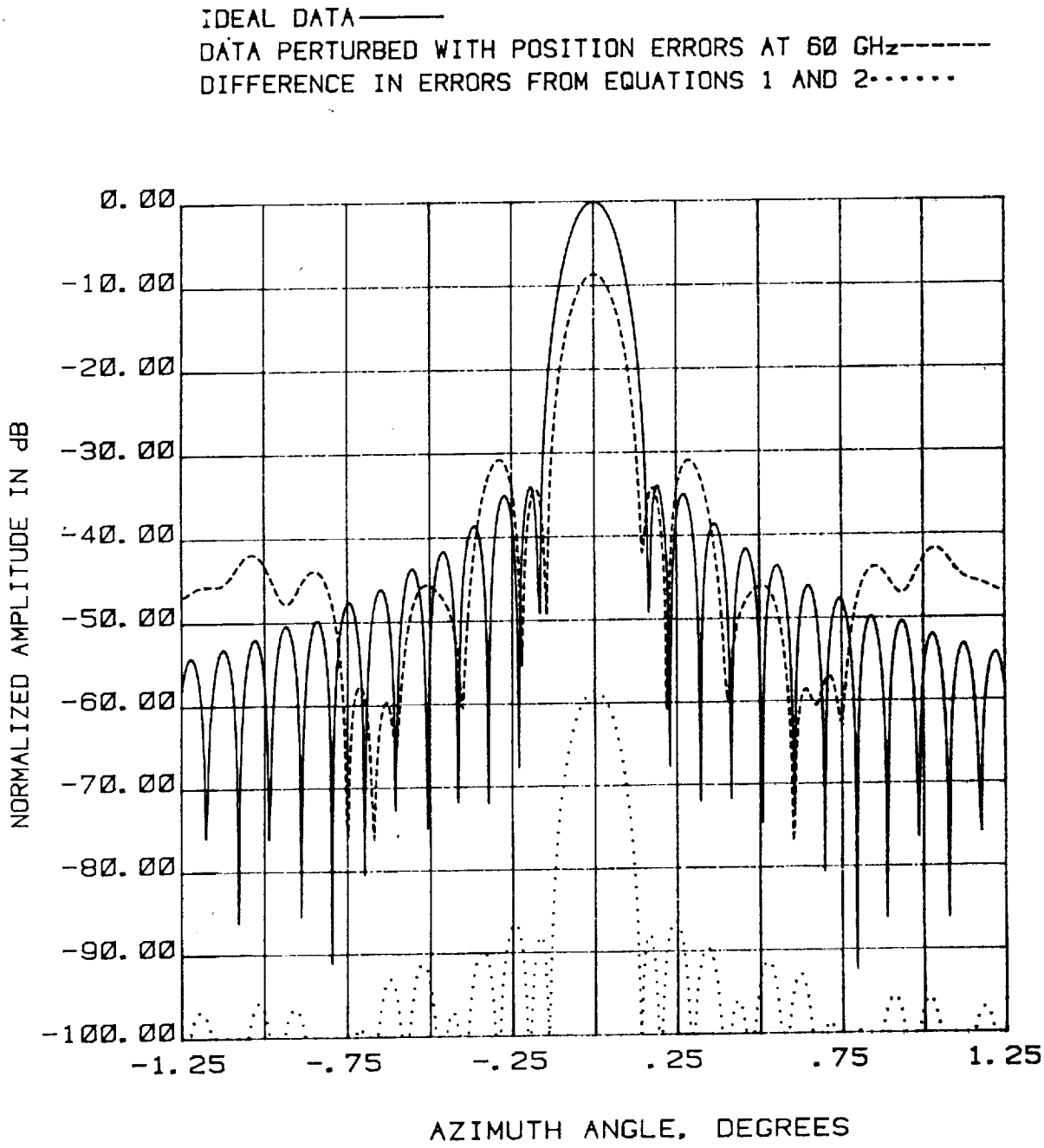

Figure 2 Effects of Positioning Errors on Far-Field Pattern

$$\frac{\delta_z^i \partial^i \overline{E}_c}{i!\,\partial z^i} = \sum_{k_x=-\infty}^{\infty} \sum_{k_y=-\infty}^{\infty} \frac{\delta_z^i}{i!} jk_z^i e^{j(k_x x + k_y y)} \overline{A}_c(k_x,k_y,k_z) \tag{3}$$

$\overline{A}_c(k_x,k_y,k_z) = \overline{A}_c(\overline{K})$, the plane wave coefficient of the Fourier transform of $\overline{E}_c$

$\overline{K}$ and k_x, k_y, and k_z are wave numbers of x, y, and z ,for a given plane wave $\overline{A}_c$

$k_o = \sqrt{k_x^2 + k_y^2 + k_z^2}$, where k_o is the wavenumber in the direction of plane wave propagation,also the maximum wavenumber

$e^{j(k_x x + k_y y)}$ is the Fourier multiplier

j is the square root of -1

Equation 1 can also be expressed using the relationship of equation 3, the result of which is equation 4. The advantage of equation 4 is that for planar near-field measurements it can be calculated without neglecting any derivatives. The limits of equation 4 have been reduced from $-\infty$ up to ∞ to $-k_o$ up to k_o by using the fact that wavenumbers which exceed k_o will not propagate.

$$\overline{E}_m = \sum_{k_x=-k_o}^{k_o} \sum_{k_y=-k_o}^{k_o} \overline{A}_c(\overline{K})\, e^{j\overline{K}\cdot(\overline{r}+\overline{\delta})} \tag{4}$$

To determine the pattern errors derived from position errors equation 4 could be used exactly as expressed above. However, this error evaluation would require calculations proportional to n^4 (n is the size of the near-field array in one dimension), which for a reasonable size n, such as 128, results in over three billion calculations. Therefore, the assumption was made that δ_x, δ_y and δ_z were much smaller than λ resulting in an equation requiring calculations proportional to n^2 instead. Equations 5 through 7 show the steps to this asymptotic derivation.

$$\overline{E}_m = \sum_{k_x=-k_o}^{k_o} \sum_{k_y=-k_o}^{k_o} \overline{A}_c(\overline{K})\, e^{jk_o\delta_z\left(1-\frac{k_x^2+k_y^2}{2k_o^2}\right)}\left(1+j(\delta_x k_x+\delta_y k_y)\right)e^{j\overline{K}\cdot\overline{r}} \tag{5}$$

In equation 5, single term Taylor series are substituted for the δ_x, δ_y and δ_z perturbations. The assumption made in this step is that most of the fields integrated will be directed parallel to the z-axis, therefore reducing the size of k_x and k_y to proportionally small numbers and allowing a truncation of the associated Taylor series without reducing the model accuracy more than 10%.

$$\bar{E}_m = e^{j\delta_z k_o} \sum_{k_x=-k_o}^{k_o} \sum_{k_y=-k_o}^{k_o} \bar{A}_d(\bar{K}) \left(1+j\left(\delta_x k_x+\delta_y k_y-\delta_z \frac{k_x^2+k_y^2}{2k_o}\right)\right) e^{j\bar{K}\cdot\bar{r}} \tag{6}$$

In Equation 6 another Taylor series is used to remove all exponential terms with the δ_x, δ_y and δ_z from inside the summations. However, because δ_x, δ_y and δ_z are all functions of position and not constant, they must be factored outside the summations using some approximation or the error computation still results in more than n^4 calculations.

$$\bar{E}_m \approx e^{j\delta_z k_o} \left\{ \bar{E}_c + j \left\{ \begin{array}{l} \delta_x \sum_{k_x=-k_o}^{k_o} \sum_{k_y=-k_o}^{k_o} k_x e^{j\bar{K}\cdot\bar{r}} \bar{A}_d(\bar{K}) + \\ \delta_y \sum_{k_x=-k_o}^{k_o} \sum_{k_y=-k_o}^{k_o} k_x e^{j\bar{K}\cdot\bar{r}} \bar{A}_d(\bar{K}) + \\ \frac{\delta_z}{2k_o} \sum_{k_x=-k_o}^{k_o} \sum_{k_y=-k_o}^{k_o} \left(k_o^2-k_z^2\right) e^{j\bar{K}\cdot\bar{r}} \bar{A}_d(\bar{K}) \end{array} \right\} \right\} \tag{7}$$

The approximation used in equation 7 should be accurate unless the position errors exceed 25% of the sample spacing and the far-field pattern nears its peak value at angles more than 10° off boresight. For the current scanning mechanism this level of position error occurs above 300 GHz. If a angle of peak power is nearer to boresight, the error model can be used to simulate higher measurement frequencies. In cases of wider angle steering of the antenna equation 7 can be redefined to include the phase errors arising in the x and y directions as is described in equation 8. For antennas having low directivity the approximations of equations 7 and 8 will not be truly representative of the measurement errors, due to the over truncation of the Taylor series. The model will also quantify the degradation with frequency caused by the transverse (in-plane) position errors given the radiation pattern type of the antenna.

$$\bar{E}_m \approx e^{j\bar{K}\cdot\bar{\delta}} \left\{ \bar{E}_c + j \left\{ \begin{array}{l} \delta_x \sum_{k_x=-k_o}^{k_o} \sum_{k_y=-k_o}^{k_o} \left(k_x-k_x'\right) e^{j\bar{K}\cdot\bar{r}} \bar{A}_d(\bar{K}) + \\ \delta_y \sum_{k_x=-k_o}^{k_o} \sum_{k_y=-k_o}^{k_o} \left(k_y-k_y'\right) e^{j\bar{K}\cdot\bar{r}} \bar{A}_d(\bar{K}) + \\ \delta_z \sum_{k_x=-k_o}^{k_o} \sum_{k_y=-k_o}^{k_o} \left(\frac{k_z'^2-k_x^2-k_y^2}{2k_o}\right) e^{j\bar{K}\cdot\bar{r}} \bar{A}_d(\bar{K}) \end{array} \right\} \right\} \tag{8}$$

where k' = the direction of peak directivity

Based on equation 7, if the residue caused by transverse position errors is small, then the z-position errors can be corrected very accurately using the relationship of equation 9 , which neglects the transverse position errors. This correction will require an a priori knowledge of the z-position errors but, for highly directive antennas, will result in a greatly increased upper frequency limit on the scanner due to position errors.

$$\overline{E}_c \approx e^{-j\delta_z k_z} \overline{E}_m \quad (9)$$

Figure 3 shows how effective this correction is on the far-field pattern data of Figure 2, reducing drastic pattern errors of the first measurement to the pattern of Figure 3 with virtually no discrepancy from the assumed error free far-field pattern. The assumptions made in developing the position error model for the NFML had next to be verified by experiment to prove conclusively that the approximate form of equation 7 could be used to simulate the behavior of the test article to a millimeter wavelength signal. This verification was performed using measurements up to 18 GHz on the current task and will be performed again on the next task to upgrade the scanner to 26 GHz.

2.2 Long Term System Drift

One of the major sources of slowly varying system error is system drift. Its effect on the measured antenna pattern, in particular mainbeam and first sidelobes, can be substantial depending on the drift function and the collection mode. The least detrimental system drift is linear. For rectangular or bifurcated scanning the only error caused by linear drift is boresight alignment. For quadrant scans, linear drift can degrade the pattern, however this drift is easily isolated and removed from collected data with proper analysis.

A periodic system drift will result in an error term more difficult to isolate, however, this term can be evaluated accurately by comparing a scanned line to a stepped line of collection data. Using this technique any slow system drift will cause a discrepancy between lines collected in 10 seconds and lines created over the duration of 25% to 100% of the near-field collection. The assumption for this study, based on the ease of modeling the mathematical behavior of system drift, was that system drift could be factored out of data using post-collection processing; however, this assumption needs to be verified with any frequency upgrade of the scanner, because the accuracy of the compensation may become insufficient to satisfy measurement requirements.

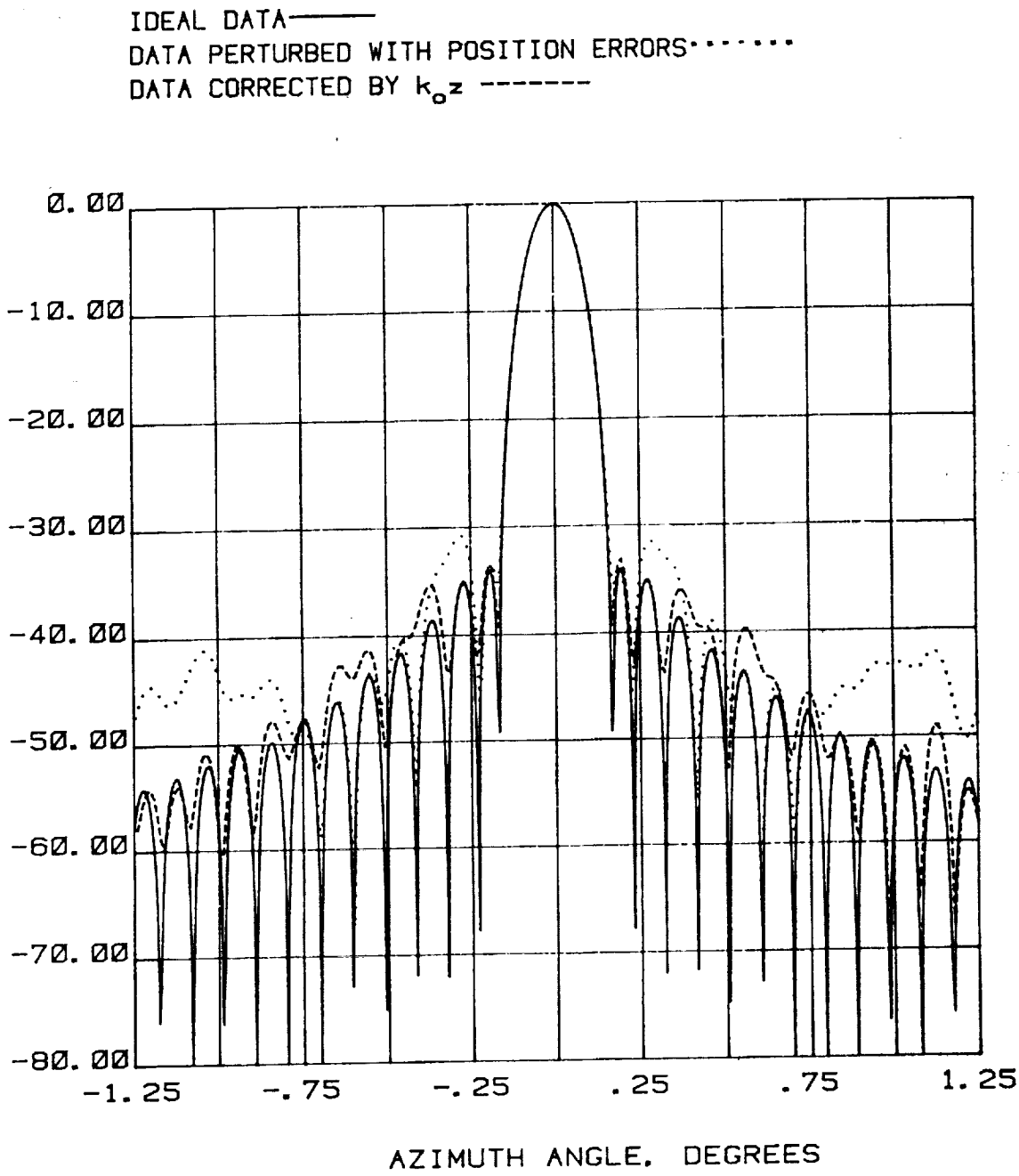

Figure 3 Correction of Position Errors using k_oz Approximation

Sources of system drift are thermal fluctuations in the environment, cable fatigue, variations in the power levels for both dc and rf biasing networks, cable heating due to flexure, and oscillator frequency drift. One of the most difficult terms to evaluate as a source of system drift are thermal fluctuations in the environment because of the complexity of the environment containing the long cable runs used to establish the phase reference. This environment includes cattracks, suspended cabling, and cabling attached to concrete floors, metal walls, and other supporting surfaces. All the mounting surfaces may have different and independently varying temperatures.

Small thermal fluctuations in the controlled environment surrounding the measurement system can cause changes in the defining parameters of system components, including the electrical length of the coax, mechanical tolerances of the scanner, even the frequency of oven regulated oscillators, and the stability of any system component. Typically, the thermal variance of the component is a negligible error term in the final data. However, it is unusual to characterize component stabilities over the narrow temperature band of metrology laboratories, and for some components may cause wrong assumptions about component stability. One case is the semi-rigid coax used to establish a stable phase reference for the data. Manufacturers' information is usually given for this product over ranges of 50°F or more with the assumption that changes in the electrical length of the cable are linear over smaller temperature increments. Also, the experimental data is usually derived from cables shorter than 3 feet. However, a check with DuPont yielded the narrow temperature curve of Figure 4 for the cable dielectric (tetrafluoroethylene, usually called teflon) alone. Also shown on Figure 4 is the expansion coefficient region of the metals commonly used coaxial cables, copper, steel, bronze, and silver. The most rapid change in linear expansion is 439 microinches/inch/°F, which occurs at laboratory temperature (DuPont data specifies a transition state at 66° F), and may be more rapid over a narrower temperature range. Verification of the dielectric behavior in semi-rigid cable is difficult because of the fractional degree thermal sensitivity. If this expansion value is assumed correct for solid dielectric cable, it results in a path length change of 0.26 inches (6.7 mm) for a temperature differential of 1°F between two 50 foot (30.5 meter) cable runs, at 100 GHz this change would be 2.2 λ, an almost uncorrectable error. The duration of a typical collection, 1 to 5 hours, could allow a temperature drift of 0.1°F, even in a temperature controlled cleanroom, between the test and reference cables, which would account for most of the drift observed in system. Figure 5 shows typical drift due to instrumentation alone. Experiments, described in sections 3.3 and 3.4, determined that the long cable lines were the primary sources of system drift.

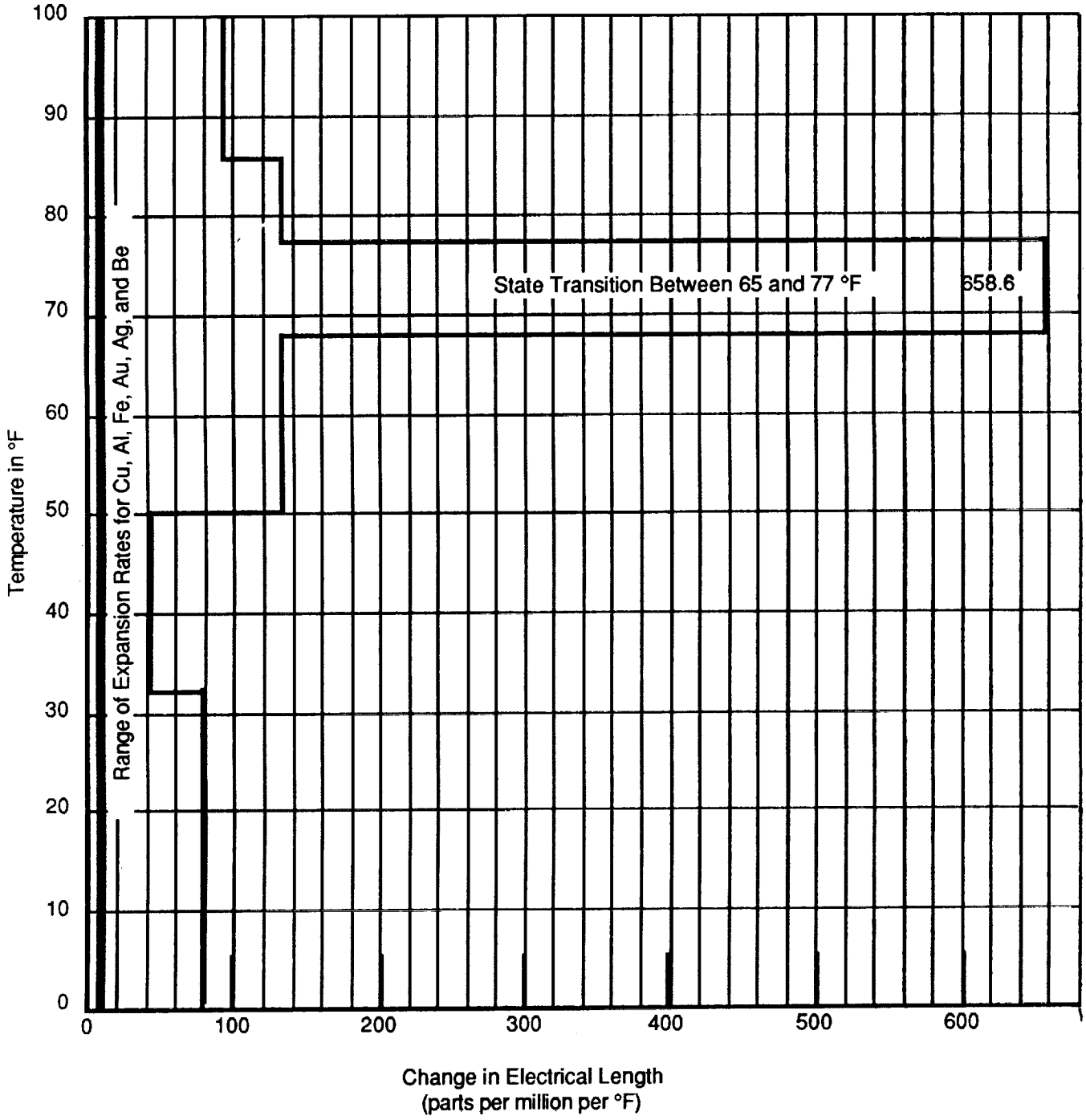

Figure 4: Thermal Expansion of Coaxial Cable Materials

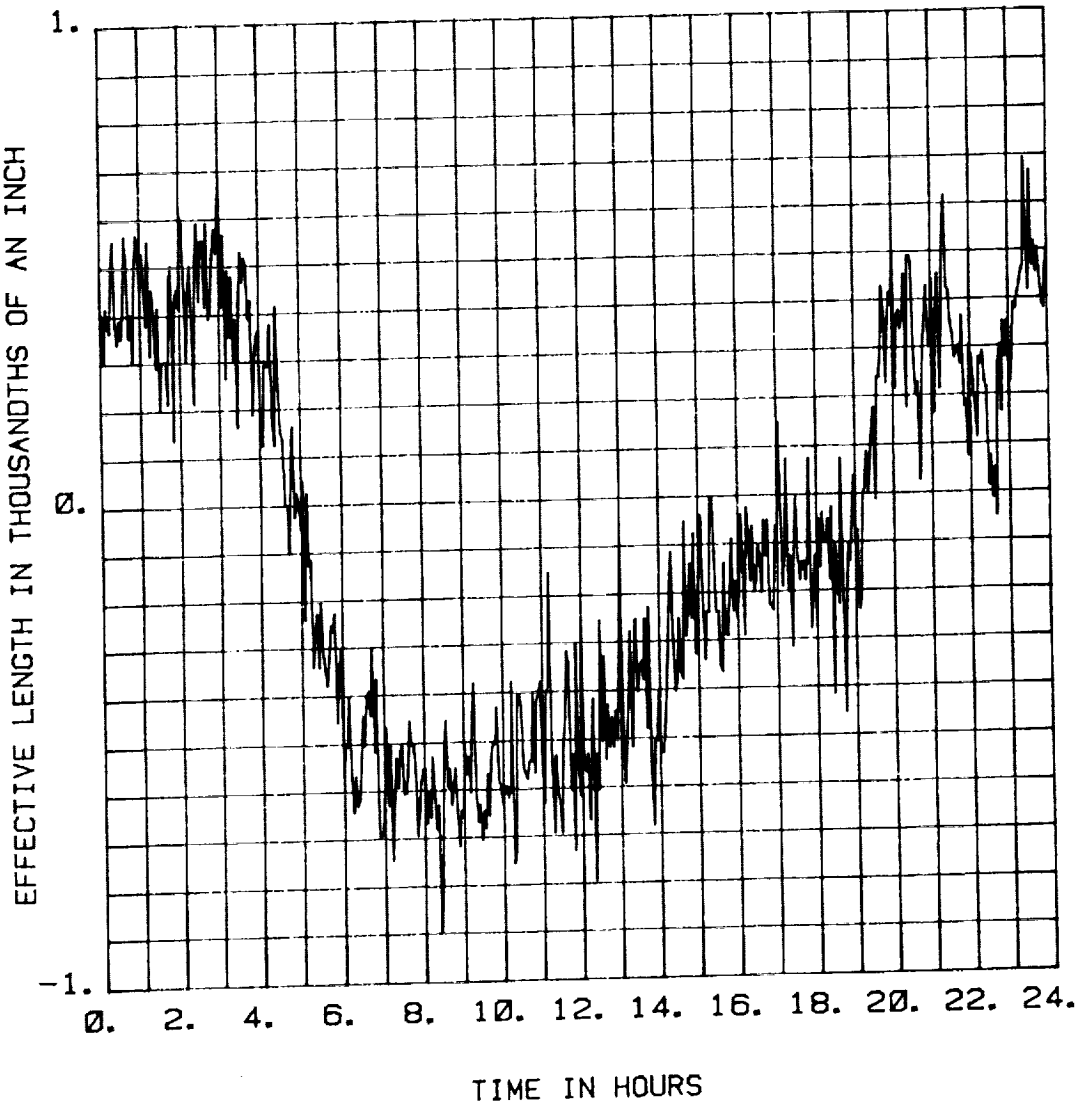

Figure 5 System Long Term Drift, Instrumentation Only

2.3 Quadrant and Bifurcated Scanning

The various collection modes used at the NFML add complexity to the error model, in particular quadrant scanning causes symmetry in the collection errors that must be considered for any aperture exceeding 20 feet (6 meters). Figures 6 and 7 show the effect of using each scan geometry on the contour pattern of a typical antenna. Although a quadrant scan can have some errors removed in the post collection data processing, the accuracy of this compensation may not be sufficient to maintain a high quality system. Table 2 shows the errors in several antenna parameters resulting from quadrant scanning and the improvement expected with post collection processing. Based on these results quadrant scanning to produce acceptable pattern data in excess of 60 GHz appears difficult. One possible method to eliminate the quadrant scan errors is upgrading the scanner to collect 42 feet (12 meter) apertures in bifurcated mode. This upgrade would also simplify the analysis of any drift components and reduce the collection time by 50% further reducing errors from system drift.

Table 2: Summary of Error Parameters for the Non-Rectangular Scans

Error Term	Magnitude of Error*	
	Uncorrected	Tilt Corrected
Directivity and Gain	-0.77 dB	-0.30
Half-Power Beamwidth	4.2%	2.3%
Peak Sidelobe (approximately -30 dB)	6 dB	3 dB
Sidelobe Envelope	0.18 dB/dB	0.10 dB/dB
Electrical Boresight Position	±0.005°	±0.001°
Aperture Phase Tolerance (RMS)	±0.018"	±0.008"

*A scanner positioner RMS of 0.01 inches was assumed for this model of a 10 meter aperture with a test frequency of 60 GHz.

2.4 System Short-Term Stability

For the purpose of this study, short-term stability is defined as a type of system drift that is relatively uncorrelated over any period of time exceeding the collection of 20 data lines. This behavior is caused by any of several second order error sources, such as phased locked loop stability, thermal drift in cables due to flexure, power fluctuation of the DC power supplies, and possibly air turbulence. The errors caused by this type of source, although slowly varying, are not repeatable and are not easily isolated because of their lack of correlation. Error due to short-term drift can be reliably bounded (because its correlation function is small) by a random noise component of equivalent level. The true magnitude of this error source cannot be predicted accurately for millimeter wavelength applications until the system upgrade because of its source. However, based on the analysis of this study the error source would need to increase an order of magnitude above current experimental measurements to become a major error source.

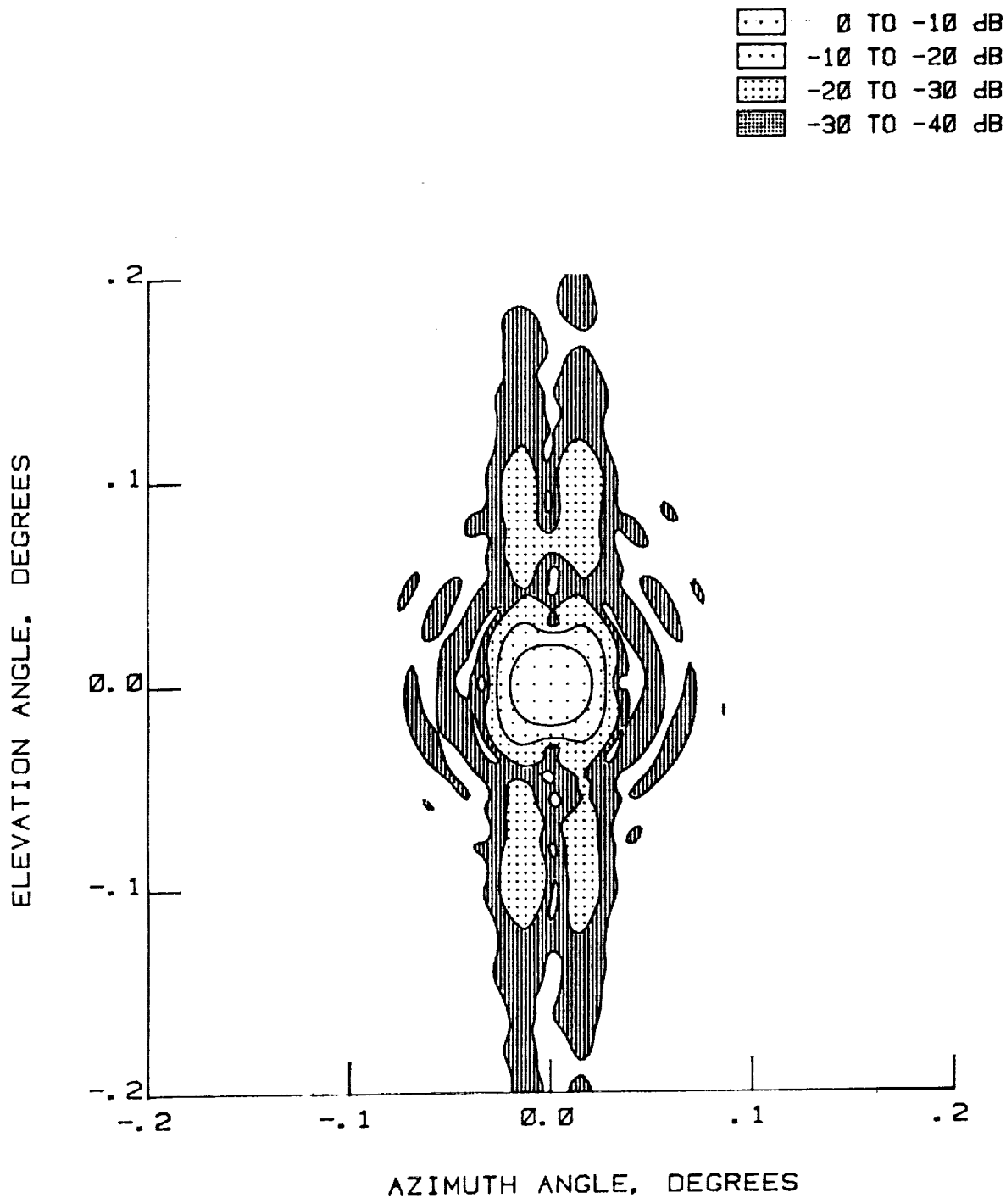

Figure 6 Far-Field Pattern Errors, Bifurcated Scan

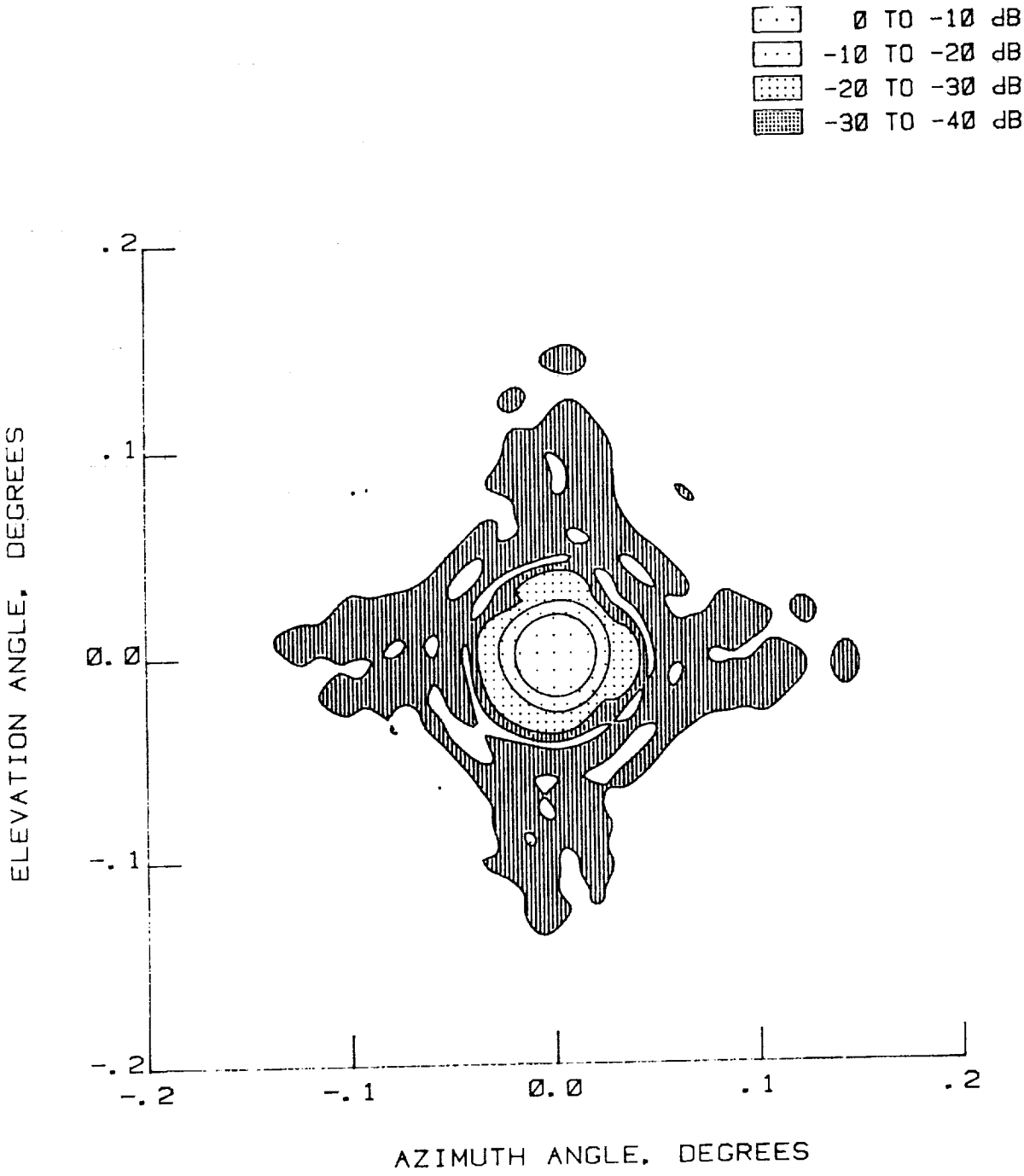

Figure 7 Far-Field Pattern Errors, Quadrant Scan

3.0 Experimentally Measured Near-Field Errors

Several experiments were performed using instrumentation available to the NFML to better characterize measurement error sources. These experiments included microwave, laser, and electronic level measurements of position errors, measurement of system drift, and measurement of phase changes due to cable flexures.

3.1 Microwave Measurement of Position Errors

We performed an experiment evaluating system response to position error at 18 GHz.(the maximum frequency of the NFML,currently). Based on laser data, existing scanner out-of-plane position errors should cause phase deviations of 7° or more from a perfect plane. To verify the error model, we needed to demonstrate agreement between microwave and laser data. Proving agreement of the two methods was crucial, if this was not established both the far-field error model and position error compensation method could not be used confidently. To measure scanner mispositioning using a microwave calibration, a method was devised to illuminate the probe with a spherical wave from a distant point source and observing phase deviations as the scanner traveled along the ways, identical to normal collections. This method would record steady-state and the vibrational modes of out-of-plane positioning errors of the scanner, although the method would not separate the two modes.

Synthesizing the calibration plane wave from the radiating spherical wave was not trivial, because the data required post-collection processing and we assumed no prior knowledge of the source phase center location. Optimizing the phase data for planarity, we located a source approximately 590 inches (14.986 m) below the scanner. Figure 8 shows the chamber configuration used for microwave planarity measurement. The data was then compensated for path length change along the scan axis, using equation 10, resulting in the phase of Figure 9.

$$\beta = 2\pi\sqrt{y^2+z^2} + \alpha \qquad (10)$$

β = phase (in radians) of plane wave corrected for distance

y = y-axis probe position (in λ) with the source as the coordinate system origin

z = minimum distance (in λ) from source to the scanner

α = phase (in radians) of collected data at the point (y, z)

We performed further measurements, and altered the test configuration to bound effects from various parameters in the measurement. The parameters altered include frequency, source position, system microwave power, system bandwidth, source antenna and scan speed. None of these parameters were found to alter the trace in Figure 9 significantly. During processing data for Figure 9, we found three significant error components. These components were multi-path reflections, probe balancing of the multiple probes, and dependence of the phase centers on frequency. Multi-path reflections caused most uncompensated measurement errors, due to their rapid spatial fluctuation. We reduced the multi-path error component by summing results from multiple source positions, thus treating the rapid fluctuations as noise. -40 dB is the maximum multi-path reflection level allowed for a system resolution of 0.002" at 18 GHz. A problem with the microwave straightness measurement is it removes scanner tilt and quadratic bow from the final data. The removal results from collecting data without prior knowledge of the source position. To compensate for the phase curvature resulting from a spherical wave of the source requires minimizing equation 11.

$$\delta\beta \approx 2\pi\left(\frac{\delta yy}{z} - \frac{\delta yy^3}{2z^3} - \frac{\delta zy^2}{2z^2}\right) \tag{11}$$

$\delta\beta$ = change in phase due to dislocation of source from the coordinate origin

δy = dislocation along the y-axis in wavelengths

δz = dislocation along the z-axis in wavelengths

This minimization is not optimum because the cubic and linear terms are not independent. Equation 11 shows the remainder using the spherical wave assumption for correcting the measured phase. Equation 11 also can not compensate for the source not being a point. Minimizing $\delta\beta$ results in the smallest rms value of the phase, therefore the phase data will be optimum and not always the true condition. To find the true condition of y-axis, further information will be required for verification of the initial microwave data. Several methods exist to determine if the y-axis has tilt or quadratic bow, one method would be recalibration of the scanner after a drastic movement of the microwave point source to isolate the quadratic bow. Another method is using a sight level to verify tilt to gravity and any systematic bowing of the ways. A third method uses the laser to verify if there is a bow independent of the optimum microwave data. The next section will discuss correlation between laser and microwave straightness data on y-axis.

3.2 Comparison of Laser and Microwave Straightness Measurements

The next phase of experimentation determined whether the method of section 3.1 yielded results that were correlated with laser straightness data. Verification of the microwave straightness measurement was important because it would validate the model predictions for pattern accuracy based on perturbations of the near-field data. Possible sources of reduced data correlation between microwave and laser data would be chamber reflections, scanner positioning repeatability, and cable flexure. Figure 10 shows the correlation that was observed in the straightness data obtained by the two methods. Only the rms value of the two measurements appears to correlate. This is probably because for the high resolution required on the microwave data at 18 GHz, the straightness measurement may still be obscured by measurement errors. The resolution required at 18 GHz is less than 1°, this accuracy corresponds to a signal to error ratio exceeding 40 dB. At 26 GHz, this ratio reduces to approximately 37 dB, this should increase the correlation between the two measurement methods by 50%. Note that the rms measured on y-axis by either laser or microwave is still more accurate than a reflector surface rms of l/50 at 100 GHz.

3.3 System Stability Using Current Instrumentation

System long term stability should be directly proportional to frequency. Stability is essential to near-field measurements over long time periods, a day or more, because if the system signal drifts more than several degrees and hundredths of a dB obtaining an accurate measurement may become nearly impossible. Figure 11 is a trace of the signal phase over a 12 hour period given in inches of electrical path length. If this phase scales with frequency then at 60 GHz (λ = 0.2 inches or 5 mm), accurate measurement of a l/50 reflector surface would require a rms value for uncorrectable drift of <0.002 inches (50 microns) to reduce the uncertainty of the surface measurement to less than 4% (0.2 dB). Therefore, for phase drift of the magnitude observed below a compensation will be required.

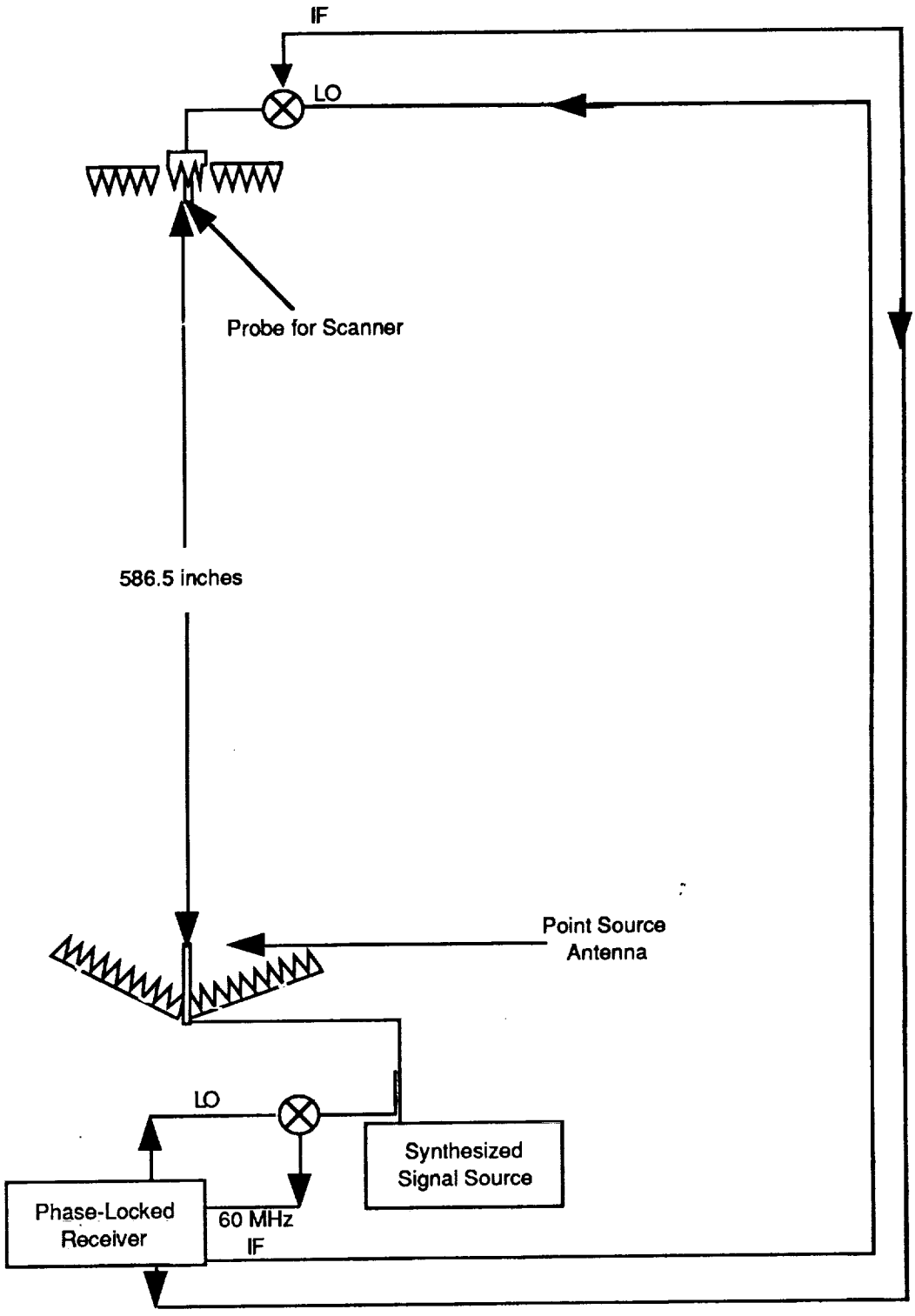

Figure 8: Microwave Straightness Measurement Circuit

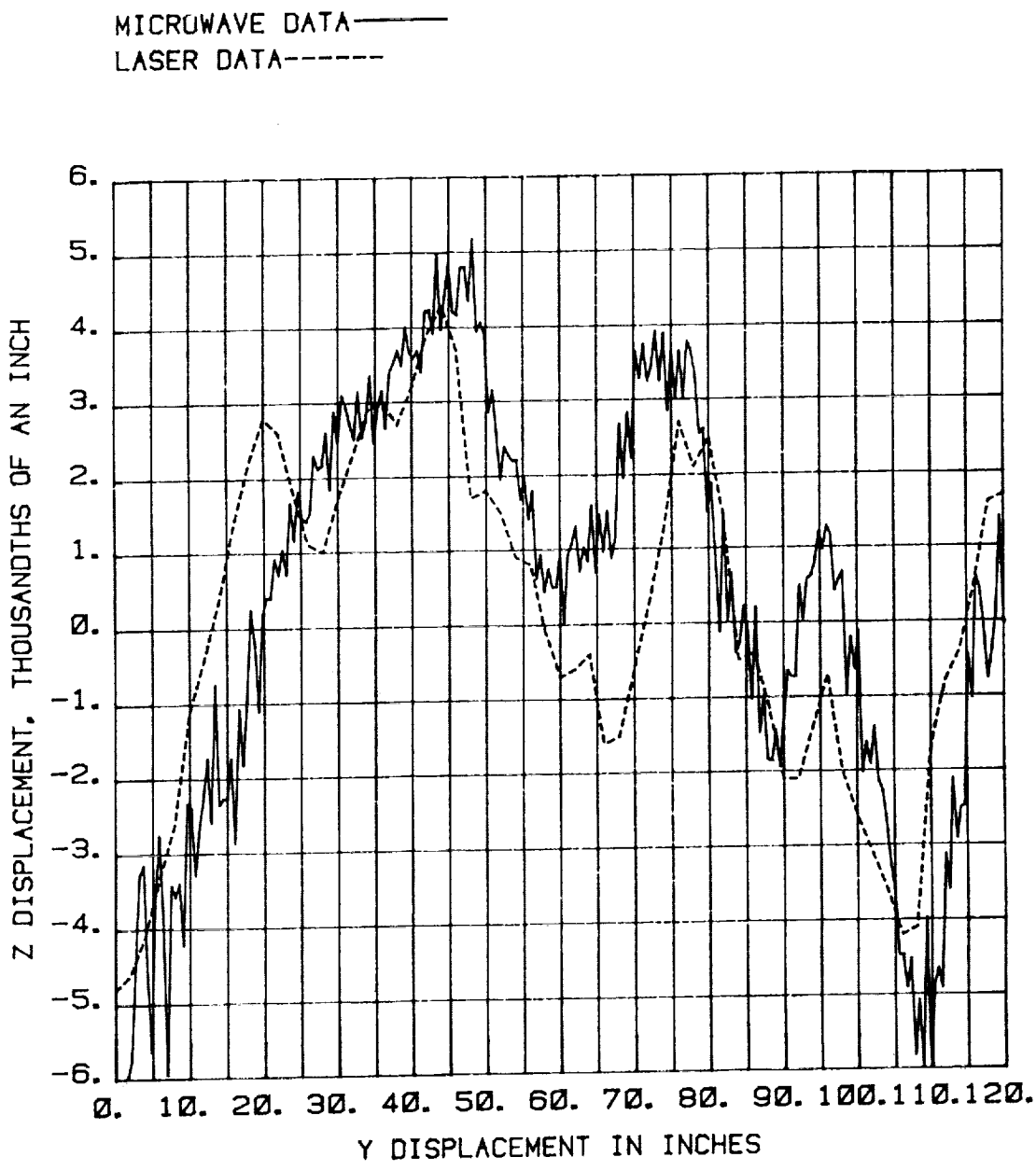

Figure 9 Microwave Straightness Data

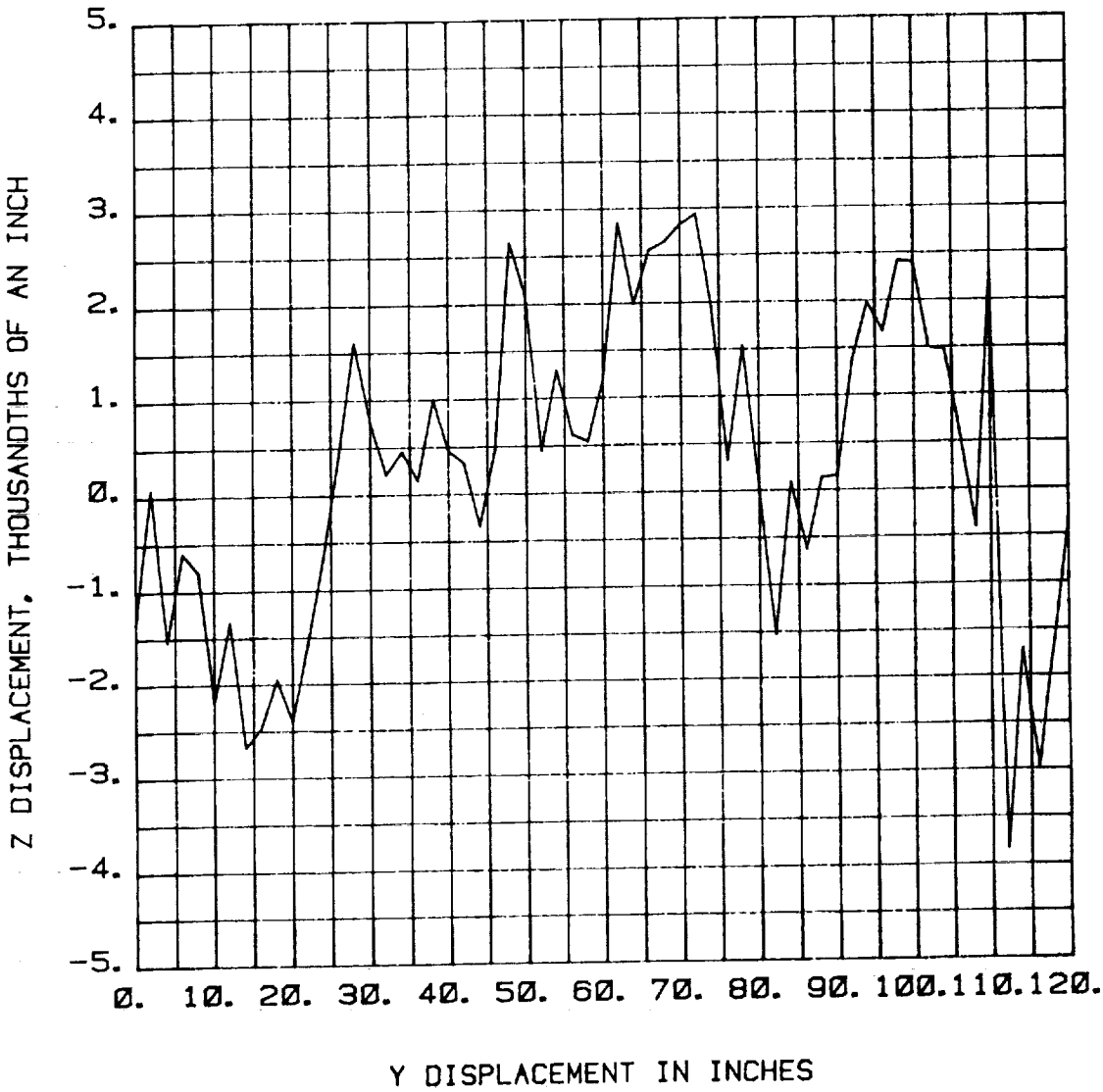

Figure 10 Correlation of Laser and Microwave Straightness Data

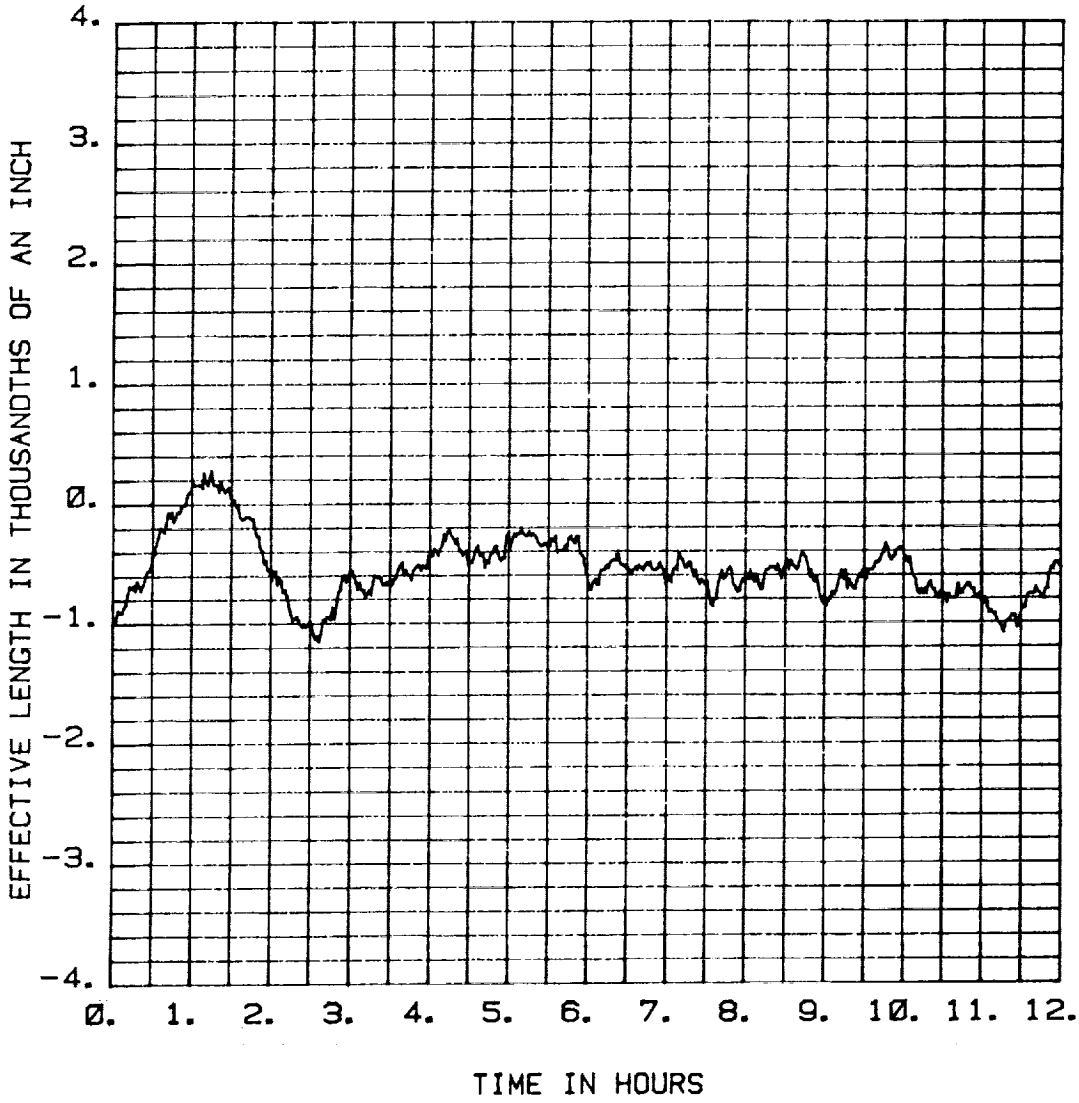

Figure 11 System Long Term Stability with Current Cabling

3.4 Cable Flexure

Measurement of electrical phase at millimeter wavelengths is extremely sensitive to cable flexure, because flexure directly perturbs the physical length of the cable. For planar near-field measurements, cable flexure is inherent in the scanning technique. To minimize the total effects of cable flexure, the NFML has matched the length of the test and reference channel approximately, and uses coiled cable at all pivot points to reduce plastic bending of the cables. Plastic cable bending is the permanent deformation of the cable which occurs with each flexure cycle. However, the coil method does not guarantee reduction of second order errors from cables due to thermal gradients, varying stresses, variance in performance by lot, and aging. We evaluated the magnitude of these second order effects experimentally in the most stressed section of the system.

The most highly stressed section of cabling at the NFML is the cable running through the x-axis cattrack and rotary table. This cable is plastically bent and unbent with a deformation of over 0.01" possible at least once every collection. In this experiment, two 80 foot cables were configured identically and the relative phase recorded during a mechanical cycle of the cattrack. Figure 12 shows the data from this experiment. The phase did not remain constant between the 80 foot cables during flexure. Thus, second order errors may be even larger than the observed deviations of this experiment which should have yielded a zero deviation, theoretically. These results indicate that the cattrack should be modified to reduce its phase fluctuations. After determining the optimum stability of semi-rigid through the most stressful part of the scanner, next a worst case experiment was performed.

The worst case evaluation was achieved by using a path length difference of approximately 100 feet (30 meters) at a test frequency of 18 GHz between the reference and test cables and observing the change in phase between the minimum and maximum points of flexure on y-axis. Figure 13 shows the results of this experiment. Based on these two flexure experiments and the system drift evaluation, the expected phase deviation over a 4 hour test using the current transmission media may exceed 15° at 60 GHz (assume the deviation is a standard deviation of the Gaussian function, i. e. 68% chance that deviations are smaller than 15°). This deviation could result in significant measurement errors unless the stability of the transmission media can be improved.

Several improvements to the transmission media available are the following: shortening the total electrical path, better matching reference and test channel impedances and path lengths, replacing the coaxial media with a fiber optic system, and thermally stabilizing the transmission media using insulation. Research by others has shown solid dielectric cables using PTFE (teflon), like the semi-rigid 0.141" coax used at the NFML, do not change length linearly near room temperature.[3] Figure 4 (Section 2.2) shows the rapid change in volume relative to temperature of teflon. Figure 14 shows a comparison of path length stability for several transmission media versus temperature.[4]

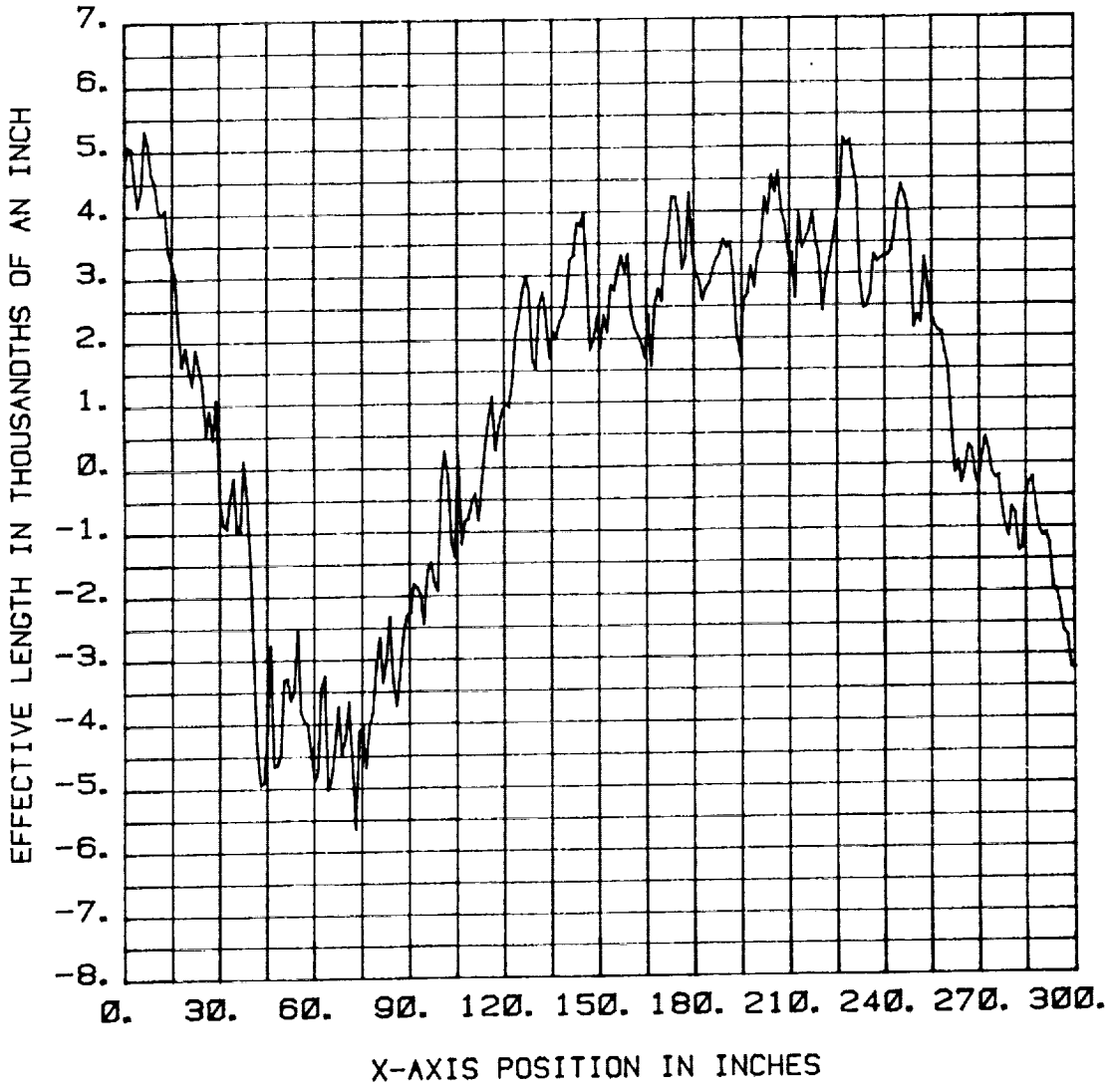

Figure 12 Phase Deviation During Flexure of Two Semi-Rigid Cables

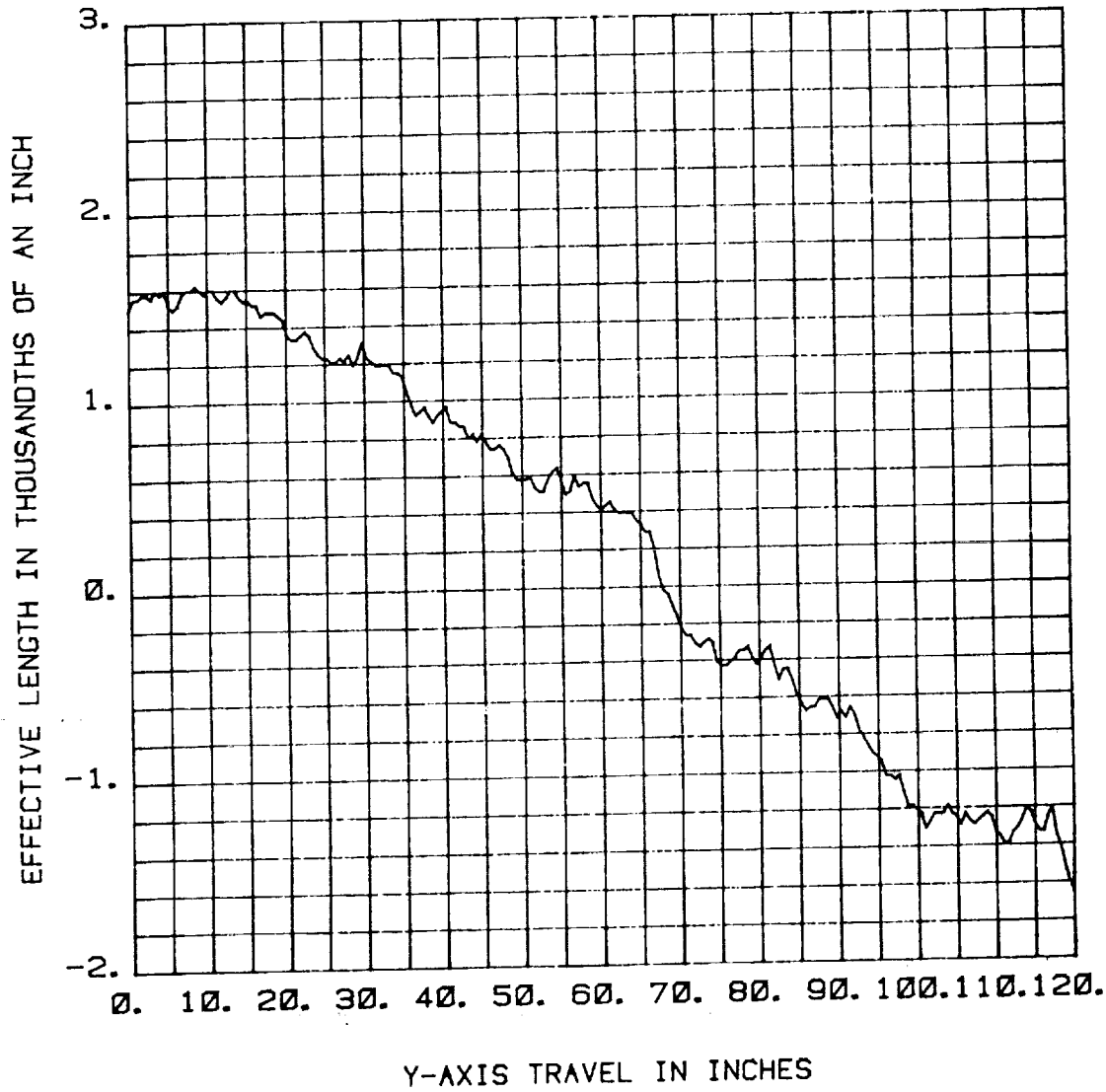

Figure 13 Phase Deviation During Flexure for Entire System Path

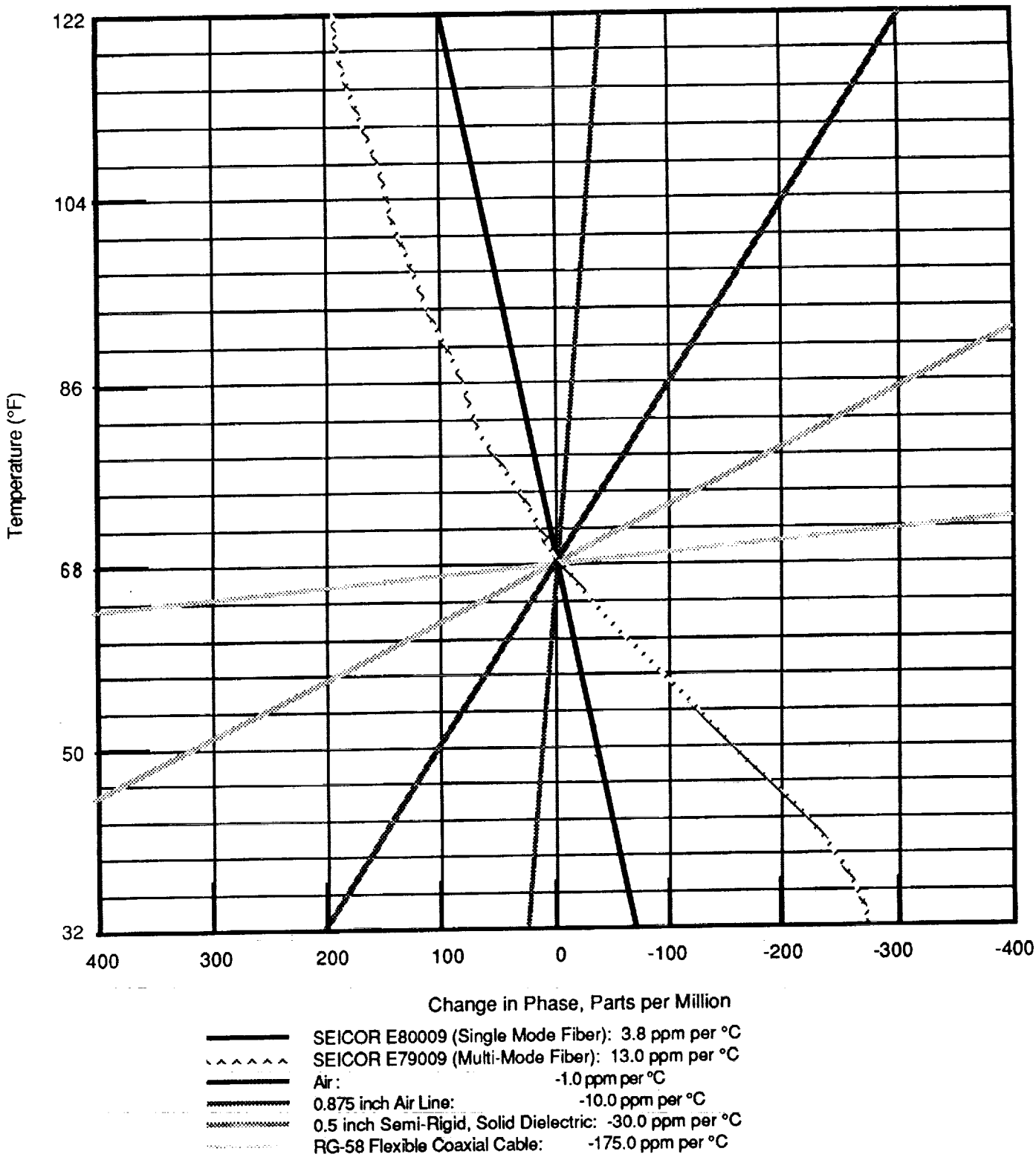

Figure 14: Path Length Versus Temperature for Various Transmission Media

3.5 System Noise Level

The system noise level is determined by the thermal noise power equation, the same equation that is commonly used for link calculations. The equation and associated terms are defined below.[5]

$$P_{noise} = \tilde{k} T_m B_m \tag{12}$$

$\tilde{k}$ = Boltzman's constant, 1.38E-20 milliwatts per Kelvin per Hertz

T_m = Measurement temperature in Kelvin (approximately 290K)

B_m = Measurement bandwidth in Hertz (approximately 3 kHz)

P_{noise} = Thermal noise power

The system is currently designed to maintain a thermal noise power level of approximately -139 dBm, however the signal to noise level observed is dependent upon the system instrumentation parameters. Table 3 will tabulate current instrumentation parameters and those of proposed millimeter systems to show the effects of component selection on the system dynamic range. Equation 13 was used to calculate the summation in the final line of the table.

$$\frac{S_7}{N_7} = \frac{G_1 G_L G_6 G_7 S_0}{(G_1 G_L G_6 G_7 F_1 + G_L G_6 G_7 (F_1 - 1) + G_6 G_7 (F_6 - 1) + G_7 (F_7 - 1)) N_0} \tag{13}$$

$G_L = G_2 G_3 G_4 G_5$, Sum of all the theoretically noiseless devices

Table 3: System Signal to Noise Levels for Current and Millimeter Systems

Signal Level (dBm)		Frequency (GHz)			
Symbol	Component	18	26	60	200
S_0	Signal Source	3	0	0	-10
G_1	Transmitter Amplification	35	35	30	0
F_1	Transmitter Noise Figure	30	30	30	6
G_2	Transmission Loss	5	10	15	0*
G_3	Aperture Gain (Inverse)**	-66	-69	-76	-87
G_4	Probe Gain	7	17	17	27
G_5	Cabling Losses	30	0	0	0
F_6	Amplifier Noise Figure	6	9	10	0
G_6	Amplifier Gain	20	30	30	0
F_7	Mixer Noise Figure	5	6	7	7
G_7	Conversion Loss	8	12	15	40
$1/N_0$	Thermal Noise (Inverse)	139	139	139	153***
	Signal to Noise Ratio	78	102	85	41

*Frequency multiplication generates 200 GHz just before the antenna input
**Assuming the aperture diameter is 10 meters
***Thermal noise is reduced by narrowing the measurement bandwidth to 100 Hz

As the table shows the signal to noise ratio of measurements decrease in direct proportion to transmitter signal amplification, however, above 60 GHz, broadband amplifiers are unavailable. Without amplification, the signal may be lost in the noise above 60 GHz. The possible solution to this problem may be designing a narrow band high power amplifier for the test frequency, although this solution would probably result in extensive development costs for the amplifier. Below 60 GHz, high power broadband sources exist, and though a 10 watt amplifier is expensive, it can be used readily for system instrumentation. Another change for millimeter is rerouting the system LO so the amplifiers and mixers will cause minimum decreases in dynamic range. By minimizing the transmission path from the probes to the mixers (frequency downconverters), the dynamic range is increased. However, repositioning the mixers will result in purchasing five mixers and four amplifiers versus two mixers and one amplifier for the current system.

Another significant term in the table is the loss due to frequency downconversion, the loss resulting from the harmonic mixing of the test signal with the local oscillator. This loss is not linear with frequency,but is dependent on the harmonic number and the efficiency and match of the mixer used. In general this loss can be reduced by lowering the harmonic number of the mixing.

4.0 Predicted Far-Field Errors at Millimeter Wavelengths

All the accuracy predictions in this section are based on the best available knowledge at the NFML without having millimeter hardware available to verify these predictions. Data used for these predictions include frequency scaled models of position errors, microwave measurements of current system performance and manufacturer information on existing millimeter components. Error contribution from a source for each parameter is approximated by a function dependent on frequency and dynamic range. Total error budget for a selected parameter will be the root sum squared (rss) total of all error sources contributing more than 10% to the total parameter measurement error. The rss total will be used because it is physically incorrect to assume that the error sources combine arithmetically. Accuracy estimates in the following sections include antenna gain, antenna directivity, boresight alignment, peak sidelobe, beamwidths, and sidelobe envelope.

4.1 Accuracy of Antenna Directivity and Gain

Antenna directivity can be determined for every near-field collection. In general, directivity is defined in a particular direction as the power ratio of the measured antenna pattern to that of an ideal omni directional antenna. In planar near-field measurements this relationship is defined by equation 14.[6]

$$D(k_x,k_y) = \frac{4\pi\Delta x\Delta y \left(\sum_{n=1}^{N} \sum_{m=1}^{M} \bar{E}(x_m,y_n)\, e^{-j2\pi(k_x x_m + k_y y_n)} \right)^2}{\lambda_o^2 \left(\sum_{n=1}^{N} \sum_{m=1}^{M} \bar{E}^2(x_m,y_n) \right)} \qquad (14)$$

$D(k_x,k_y)$ = pattern directivity at the angle defined by (k_x,k_y)

(k_x,k_y) = plane wave number

λ_o = free space wavelength of the test frequency

Δ_x, Δ_y = sample spacing in x and y, respectively

Figure 15 shows the proposed circuit to measure antenna gain for millimeter wave applications. Equation 15 is the relationship used to calculate the antenna gain. This gain value is the maximum gain for the antenna, because the equation assumes that the system is matched to the antenna.[6]

$$G(k_x,k_y) = \frac{(4\pi\Delta x\Delta y)^2 |s_{21}^{at}|^2 |1-\Gamma_a\Gamma_t|^2 \left(\sum_{n=1}^{N} \sum_{m=1}^{M} \overline{E}(x_m,y_n)\, e^{-j2\pi(k_x x_m + k_y y_n)} \right)^2}{|a|^2 \lambda_o^4 \Gamma_{p_{eff}} |1-s_{11}^{at}\Gamma_l|^2 |1-s_{22}^{at}\Gamma_l|^2 \left(1-|\Gamma_a|^2\right)} \qquad (15)$$

$G(k_x,k_y)$ = gain of the test antenna in direction (k_x,k_y)

a = system substitution loss using the two antennas in place of the attenuator

s_{11}^{at}, s_{21}^{at}, and s_{22}^{at} = attenuator S-parameters

Γ_a = reflection term for antenna

Γ_t = reflection term for the transmitter port

Γ_l = reflection term for the load (receive port)

$\Gamma_{p_{eff}}$ = effective gain of the measurement probe

Accuracy of antenna gain depends most on three factors, an attenuation standard, system stability, and repeatability of the substitution loss measurement. Each of these error components are independent because they are created by different physical characteristics of the measurement system. Effects of each component must be minimized for optimal performance. Past experience has shown the most critical device to insure system linearity is a well-behaved attenuation standard.

A rotary vane attenuation standard is used for most millimeter applications, its advantages include low VSWR, long term stability, and insensitivity to most environmental factors (including the particular vane used, temperature and signal power). The vane attenuation is proportional to the cosine of the angle between the waveguide polarization and the vane, therefore accuracy and repeatability of the rotary mechanism are critical unless the vane is locked. Measuring substitution loss of a typical millimeter antenna will require a large attenuation value, thus the calibration should use a locked vane attenuator to eliminate positioning uncertainty. If an accurate 50 dB attenuation level is required to avoid system saturation during the substitution loss measurement, then for 0.1 dB precision, the angle must be repeatable to 2.5 arc seconds (11.5 μrads). However, if the attenuator is locked prior to the near-field collection, then the uncertainty of the attenuation used in the substitution loss measurement becomes the connector repeatability, and the initial calibration. This locked attenuator will be placed between ports 1 and 2 in Figure 15, with the true position of the ports determined by the final hardware configuration. The uncertainty in the attenuation standard using this technique will then be the accuracy of the derived standard,which is less than 0.004 dB/dB or 0.2 dB for an attenuation value of 50 dB.

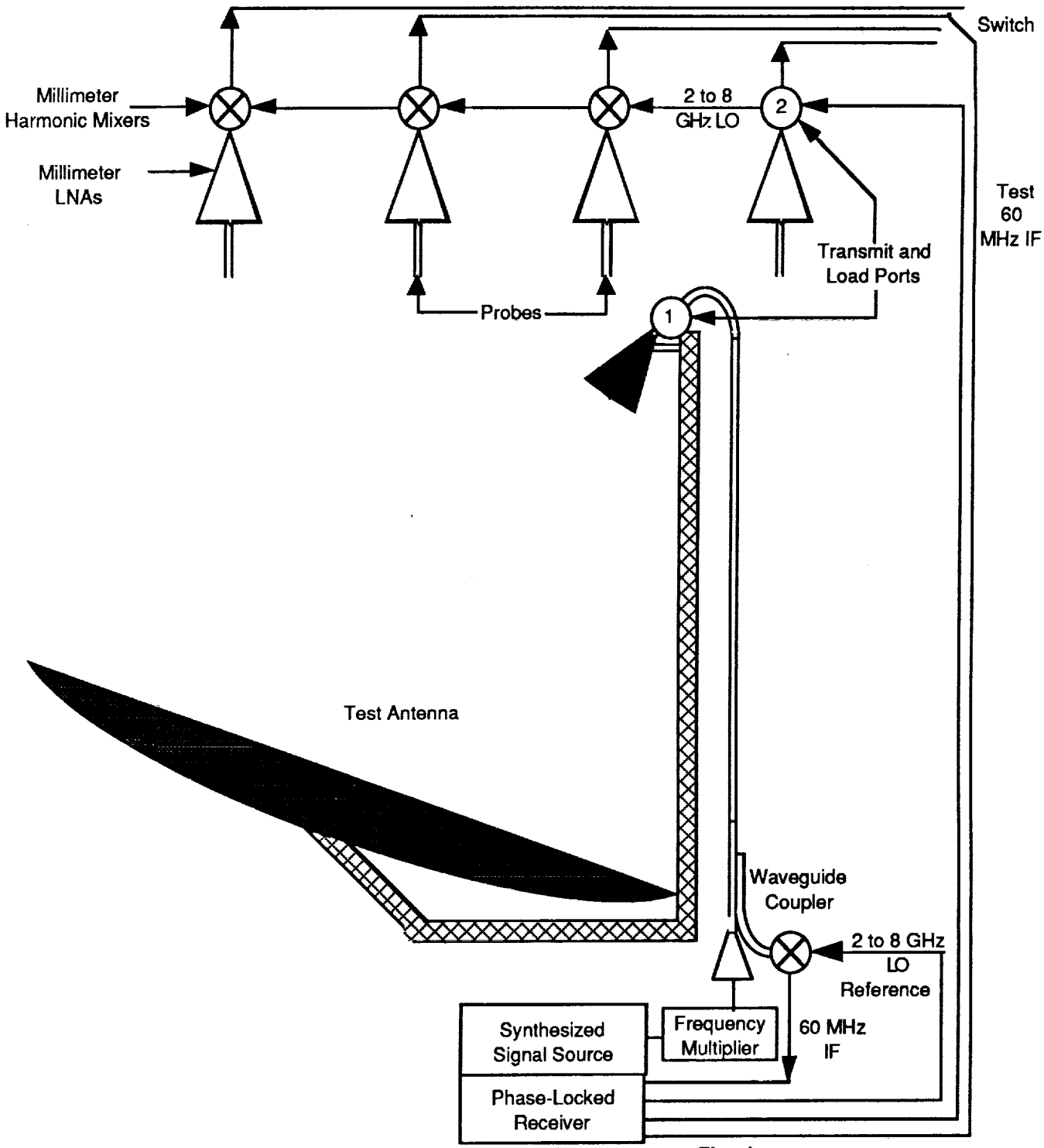

Figure 15: Antenna Parameter Measurement Circuit

The following table lists the predictions based on millimeter wave system simulation at 18,26,60 and 200 GHz. Included in the simulations are estimates of both uncorrected and corrected post-collections.

Table 4: Accuracy of Directivity and Gain at Millimeter Wavelengths

	18 GHz		26 GHz		60 GHz		200 GHz	
Error Component (dB)	Uncor.	Correct	Uncor	Correct	Uncor.	Correct	Uncor.	Correct
Positioning	0.04	0.00	0.08	0.00	0.44	0.00	4.92	0.05
Connection Repeats	0.05	0.05	0.10	0.10	0.15	0.15	0.25	0.25
Mismatches	0.05	0.05	0.10	0.10	0.15	0.15	0.40	0.40
Probe Gain	0.15	0.15	0.20	0.20	0.20	0.20	0.50	0.50
Attenuator	0.15	0.15	0.15	0.15	0.20	0.20	1.00	1.00
Data Collection	0.20	0.10	0.30	0.15	0.40	0.20	1.00	0.40
Gain	0.30	0.25	0.42	0.32	0.69	0.41	5.17	1.28
Directivity	0.20	0.10	0.31	0.15	0.59	0.20	5.02	0.40

4.2 Accuracy of Beamwidth, Electrical Boresight, and First Sidelobes

The same components determine both the directivity and beamwidth accuracy of an antenna; the positioning accuracy and data collection repeatability. Note, if the mainbeam is irregular in shape as occurs in some beam synthesis applications, the beamwidth maybe hard to define, thus increasing its uncertainty even with an accurate measurement. However, with classical pencil beam antenna patterns, the primary interest of this task, directivity and beamwidth can be linked together by the following equation.

$$\Delta\theta \approx \theta\left(\sqrt{\Delta D} - 1\right) \tag{16}$$

θ = average pattern beamwidth

ΔD = linear value for the directivity uncertainty (0.1 dB = 1.02329)

$\Delta\theta$ = uncertainty in pattern beamwidth

The square root term arises from typical antenna directivities being defined by equation 17, and applying the proportionality of equation 18.[7]

$$D_{max} \approx \frac{4\pi}{\theta^2}(\text{radians}) \text{ or } \frac{129{,}600}{\pi\theta^2}(\text{degrees}) \tag{17}$$

$$\Delta D \approx 1 - \frac{\Delta\theta^2}{\theta^2}, \quad \Delta D = \frac{D_{max} + ERROR_{max}}{D_{max}} \tag{18}$$

D_{max} = maximum directivity

$ERROR_{max}$ = maximum error in directivity

Peak sidelobe accuracy can also be predicted simply from directivity by equation 19, if the major system error sources have an approximately Gaussian (non-specular) distribution.

$$\Delta PSL(dB) \approx 20\log\left(\frac{\Delta D(linear)+PSL(linear)}{PSL(linear)}\right) \quad (19)$$

PSL = peak sidelobe of the antenna pattern in dB

ΔPSL = uncertainty in the peak sidelobe in dB

If the system errors do not have a Gaussian distribution, modeling of the specific error will have to be done to accurately predict the resultant pattern error. However, most large sets of measurement data have Gaussian distributions. Because near-field data collections are automatically large data sets, the unrepeatable errors can be accurately modeled as Gaussian noise. Drift and positioning errors are correctable and can therefore be modeled by a very small function set, typically one function.

Electrical boresight of an antenna is particularly sensitive to any systematic scanner measurement errors (drift and turntable tilt), and uncertainty in the initial mechanical alignment of the antenna. However, in past experience the error of the mechanical alignment of the antenna has exceeded the scanner alignment accuracy. This behavior is usually due to the instability of the mechanical interfaces being aligned.

4.3 Accuracy of Sidelobe Envelope Measurement

The accuracy of the antenna pattern sidelobe envelope will be derived from the behavior of several error sources, which are usually Gaussian in distribution. These sources are receiver noise in the far-field pattern, scanner position error spectral distribution, and chamber multi-path. Under normal test configurations, the predominant source will be the position error spectral distribution, shown with a simulated antenna pattern in Figure 16. This term is characterized by taking a Fourier transform of the known position errors of the scanner and scaling them appropriately to overlay the antenna pattern data.

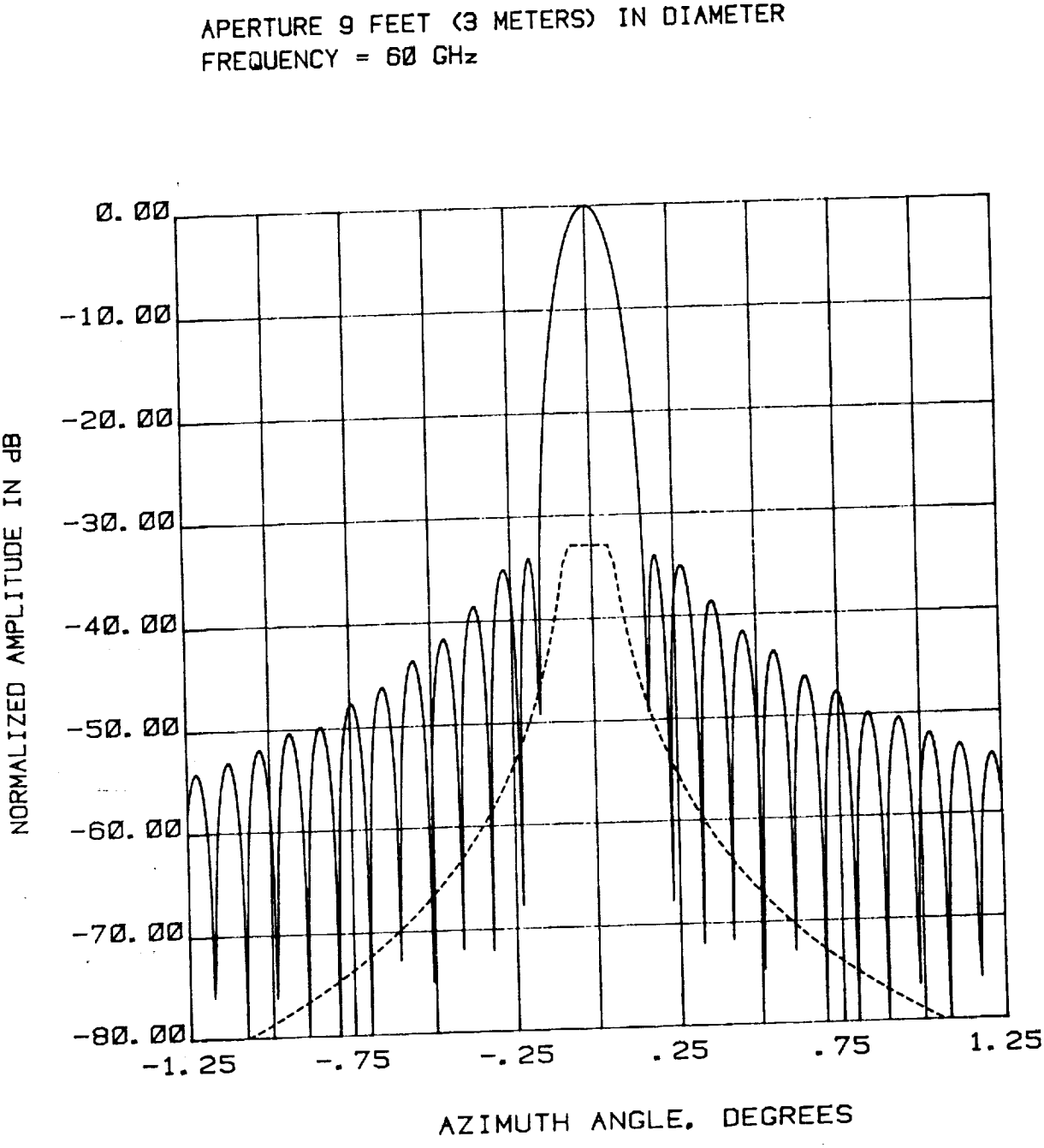

Figure 16 Measurement Errors Relative to Sidelobe Envelope

5.0 Applications of Near-Field Diagnostics at Millimeter Wavelengths

All of the diagnostic techniques developed for use in the longer wavelength bands should be equally applicable at millimeter wavelengths. Included in the diagnostic packages available at the NFML are algorithms to evaluate the electrical surface of a reflector, focus and boresight an antenna, determine the excitation of individual elements (amplitude and phase), and analyze the sources of system performance loss both ohmic and pattern. In addition to these diagnostics, the NFML is also developing several software packages to model the performance of different types of high gain antennas. Some of the models currently used at the NFML include feed array steering of reflector antennas, pattern synthesis of arrays and feed arrays, and simple blockage using geometric optics.

5.1 Electrical Surface Evaluations

For large antennas, the planar near-field measurement, excluding scattering and blockage, is proportional to the physical surface of the reflector. If physical optics model (ray tracing) is applied to the measurements, then the reflector surface is related to the electrical phase of the aperture by equation 20.

$$\delta z(x,y) \approx \delta\theta(x,y)\left(\frac{4f^2+r^2}{8f^2}\right) \tag{20}$$

$\delta\theta(x,y)$ = electrical phase in radians

$\delta z(x,y)$ = the reflector surface dispacement

f = distance from center of rotation to focal point of the reflector

(x,y) = coordinates of the vertical ray of interest perpendicular to the xy plane

$r = \sqrt{x^2+y^2}$, the radial distance from reflector center

For reflectors with large f to d ratios, the assumption can be made that $\delta z = \delta\theta/2$ with only a small error. We can then use the surface data to make precise adjustments to improve the reflector performance. The surface data has particular importance for radiometers because beam efficiency (not aperture efficiency) is a critical system parameter. The only limit to improvement of the surface accuracy is the inaccuracy of the scanner -- in particular its planarity. However, it is much easier to evaluate the scanner planarity than the surface accuracy of a reflector using currently available non-microwave measurement techniques. This simplicity is due to the ease with which the straight line travel of a planar near-field scanner can be measured versus the complexity of measuring a doubly curved reflector surface directly.

5.2 Antenna Focusing and Boresighting

After mechanical boresighting of the reflector has been established by an optical alignment, such as leveling the reflector mating interface or its edge to gravity at the NFML, the feed alignment relative to the reflector can be determined. This alignment evaluation will give accurate numbers for the optimal position for the feed based on directivity or mechanical boresight for all three positioning axes. This evaluation of optimal focusing can be expanded to include feed arrays and multiple reflector systems. Note existing methods measure electrical boresight as the discrepancy from some previously defined mechanical boresight, by using near-field measurements, the optimal electrical boresight for the antenna can be found and the mechanical system can be shimmed to compensate for the mating interface misalignment.

5.3 Array Element Excitations

Determining the pattern and excitation of each element in an array antenna is an important capability of the near-field methods. This method has long been used for optimizing planar arrays, but can also be applied to focal arrays with only minor modifications. The NFML has already developed algorithms to synthesize either optimal or arbitrary patterns from a focal feed array. These methods work well for either boresight or beam steering applications. Coma lobe reduction of steered beams will be important for radiometry applications which require beam efficiencies exceeding 90%. Figures 17 and 18 show the improvement in a far-field pattern from a single element to a 20 element array for a primary feed array steered 50 beamwidths in a reflector with a f/d ratio of 1.5 and a 2000 wavelength diameter (a 10 meter aperture at 60 GHz). Knowing the improvement possible in beam steering with a focal array is critical for making the best compromise feed design based on complexity, reliability and cost.

5.4 System Losses (Pattern and Ohmic)

One of the most basic outputs of near-field measurements is the difference between antenna directivity and gain. This difference derives from several loss mechanisms that can be determined independently using near-field measurement diagnostics. The most significant loss mechanisms are defocusing, feed spillover, ohmic losses of the feed and reflector current carrying surface, the cross-pol fields, and reflector surface imperfections (including roughness and leakage in the case of a mesh surface). The near-field measurements allow each of these loss terms to be evaluated separately, thus allowing the designer to assign priority to the reduction of each source of system loss. Also, for many large antennas, these terms cannot be evaluated accurately by methods other than near-field measurements.

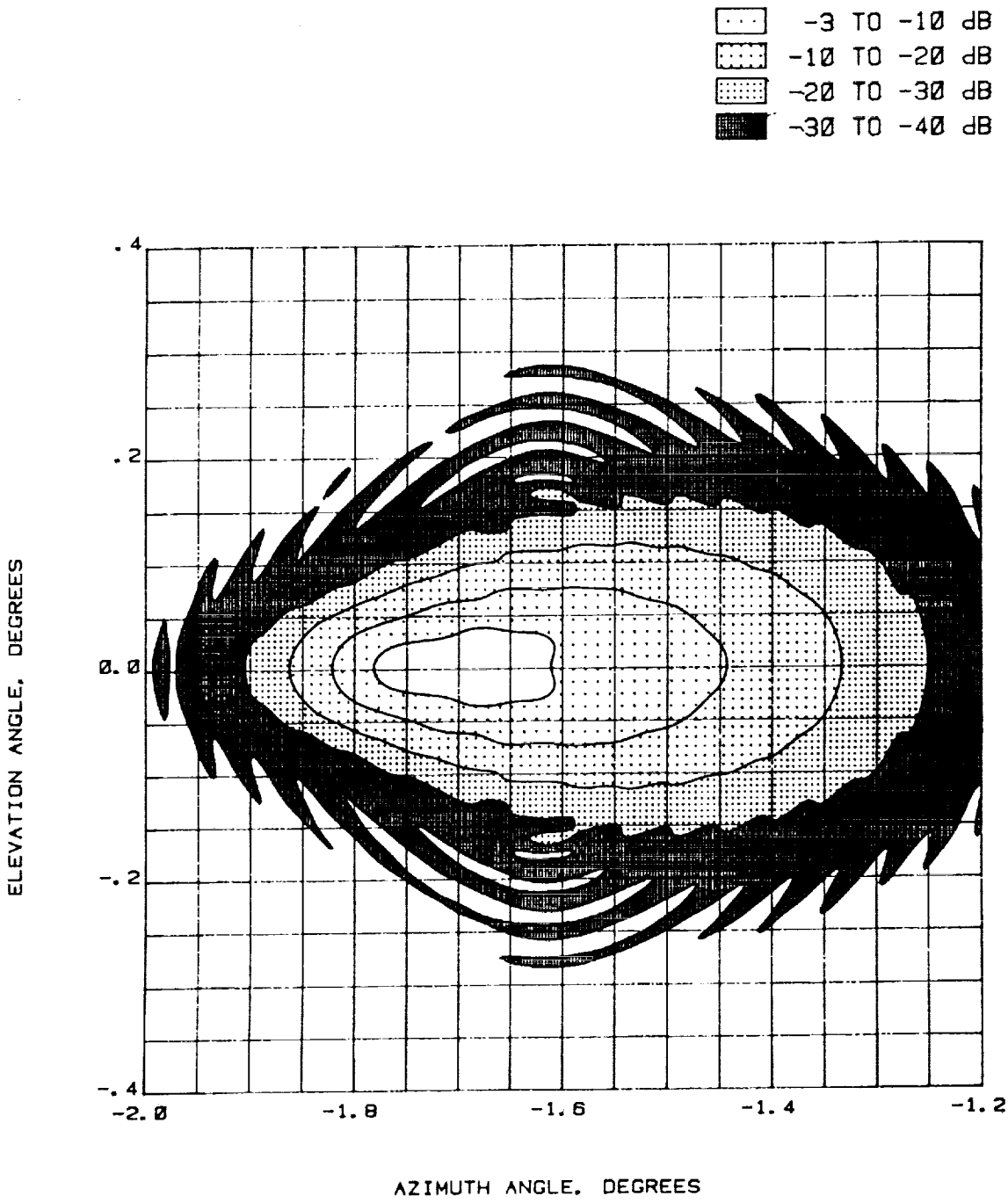

Figure 17 Secondary Pattern of Reflector Using Single Element

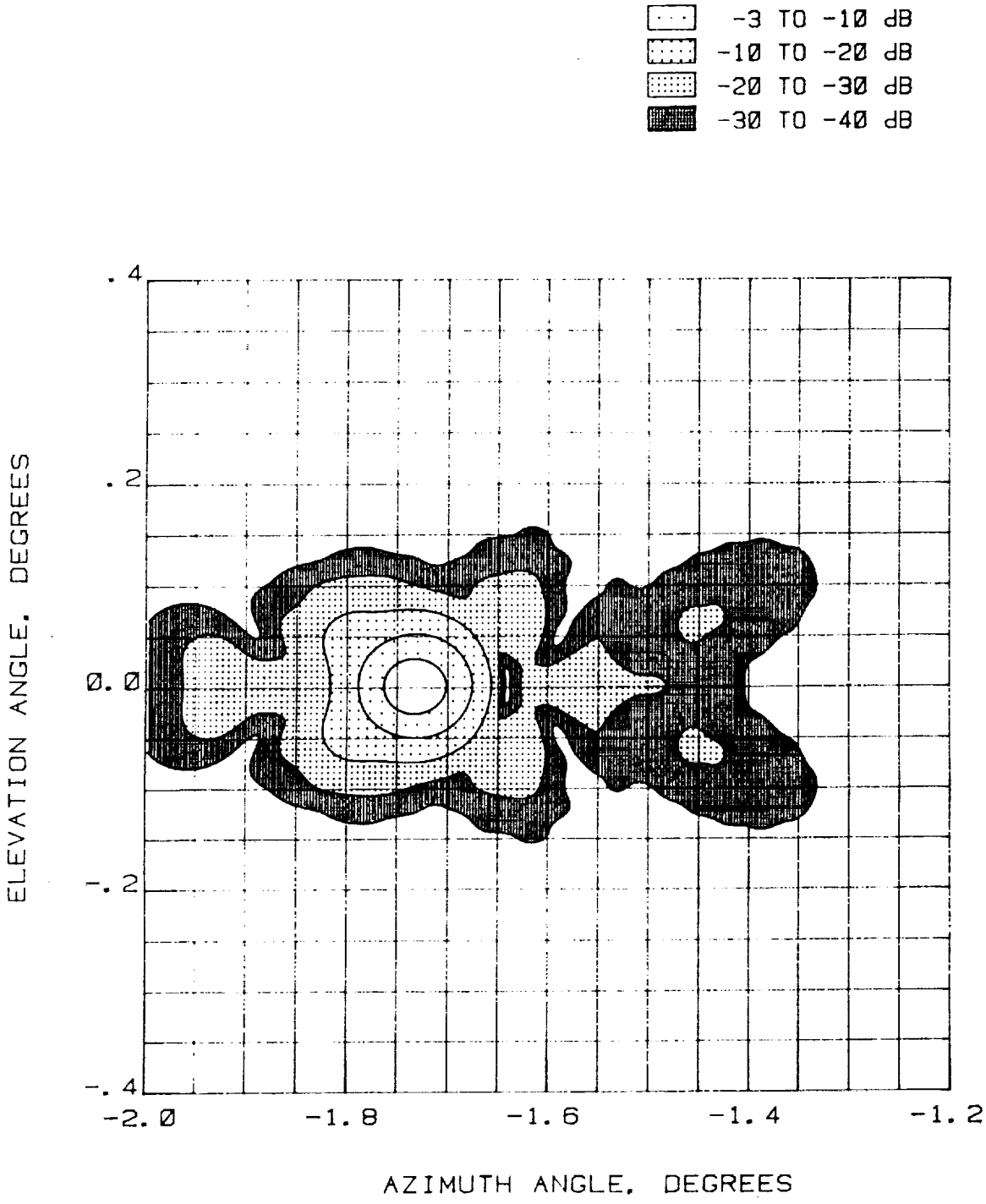

Figure 18 Secondary Pattern of Reflector Using Steered Feed Array

6.0 Cost Estimate for System Upgrade to Millimeter Wavelength Measurements

Cost estimates of configuring the NFML for higher frequencies are discussed in this section. The estimates include predictions on labor for facility reconfiguration, new fixturing requirements, facility recalibration and manufacturer's list prices (as of September 1, 1989) for millimeter wave hardware needed for the facility reconfiguration. In all the examples proposed below several options have been specified, these options are the following.

1. Full S-parameter measurement capability up to a specified frequency
2. Full S-parameter measurement capability in a waveguide band
3. Pattern measurements at a single frequency

Obviously, option 1 will be most expensive if hardware is the only consideration. However, option 1 has features that could easily reduce its final cost. Option 1 substantially lowers the risk to the program if test article frequency requirements change at an intermediate development phase. The option also permits the facility to increase operating frequency gradually, giving staff time to gain experience in large aperture millimeter wave measurements. This experience may result in utilizing less costly hardware than initially planned. Also, if the laboratory performs all calibrations on-site, it reduces the uncertainty of the antenna measurements and ensures that measurements are derived from standards that are documented in the reported results. The capabilities developed by option 1 will also allow the evaluation of subsystem components if any anomaly is found in the test article and may also be useful in the development of the subsystem components.

By comparison to option 1, option 3 will have minimal initial hardware investment, but will also result in the highest technical risk. The risk will also increase rapidly as frequencies move above 60 GHz, because no near-field facility has experience above 60 GHz. Also many components are either extremely expensive or unavailable above 60 GHz, including sources (fundamental frequency synthesized with output power exceeding one watt), mixers, measurement standards, and broadband signal amplifiers. The failure of any of these components during the measurement program could result in excessive schedule delays with the possibility having to reselect the components due to unacceptable performance.

The following sections will quantify anticipated hardware and labor requirements to perform measurements in any of the millimeter bands currently having the required components available as manufacturer specified parts. Labor costs may include any of the following activities: software modifications, tooling fabrication, development of calibration procedures, performing system error analysis, reconfiguring system components and documenting upgraded system performance. This information is for technical use only and shall not be used as a binding cost estimate for any program.

6.1 Upgrade to 26.5 GHz

Upgrading the facility to 26.5 GHz is the next obvious step in a methodical advance of the facility into the millimeter wavelength band. Obvious advantages in doing this upgrade before any other investigation of millimeter wave measurements are minimal cost, quick verification of error model at frequencies that increase many of errors by 45%, and minimal impact to current facility operations. The following list of components are needed to upgrade the facility to 26.5 GHz, and because no significant difference in cost exists for options 1 through 3 in this case, this estimate will not specify the option.

Table 5: Hardware Cost Estimate at 26.5 GHz

Component	Quantity	Cost(K)
Absorber Material	6	0.3
Mixers (SMA Connectors)	5	3.3
60 MHz PIN Switches	5	0.4
Standard Gain Horns	5	1.6
Waveguide, and Flanges	na	0.4
Waveguide Coupler	2	0.6
Load, Attenuators and Short	2	0.3
30 GHz SMA Connectors	25	0.2
Waveguide to SMA Adapters	10	1.1
Hardware Total	na	8.2

Following receipt of hardware listed above, we will evaluate the facility performance by measuring a large aperture antenna. The following table predicts the labor hours required to perform a facility calibration and error evaluation in this frequency band.

Table 6: Scanner Calibration at 26.5 GHz

Task	Hours
Probe mounting and calibration	80
Evaluation of the Scanner Alone	320
Mounting of large aperture antenna	160
Microwave measurements	280
Error Analysis	160
Report on System Performance	200
Labor Total	1200

Completion of the above tasks should provide sufficient data to accurately predict the facility performance up to 60 GHz, because upgrading to 60 GHz should only cause an approximate doubling of facility errors experimentally measured at 26.5 GHz. Also, the 26.5 GHz upgrade would make possible the capability to measure antennas with directivities exceeding 70 dB, corresponding to a half-power beamwidth of less than 0.06° (1 milliradian).

6.2 Upgrade to 60 GHz

Upgrade of the NFML to 60 GHz will require modifications to current instrumentation. These modifications include waveguide harmonic mixers, a millimeter wave source up to 60 GHz, attenuation and phase standards, and a reliable method of correcting scanner positioning errors. Due to the losses in coax at higher frequencies (greater than 1 dB per foot or 3 dB per meter), most of the millimeter components will have to be in waveguide. Some coaxial components are beginning to be produced that perform up to 60 GHz, but they are still expensive and narrowband. Under conventional waveguide designations, the frequency spectrum from 26.5 to 60 GHz is covered by three waveguide bands, Ka, Q, and U. The Ka band uses WR28 waveguide from 26.5 to 40 GHz, Q band uses WR22 waveguide from 33 to 50 GHz, and U band uses WR19 waveguide from 40 to 60 GHz. The frequency bands approximately cover the range from 1.25 f_c to 1.9 f_c , where f_c is the TE01 cutoff frequency of the waveguide. The system cost was estimated based on using purely waveguide components and covering Q-band using waveguide transitions from Ka and U band. Option 2, a single waveguide band estimate, is for U-band (Ka band would cost less).

The most costly component of accurate, broadband measurements from 26.5 to 60 GHz may be maintaining good dynamic range. Although high power sources exist for frequencies well in excess of 60 GHz, for the broadband systems of options 1 and 2, the power of the source either drops drastically or the cost of the source increases exponentially. An example of this cost increase is the change in price of a full band, 10 watt TWT at Ku versus Q-band, an increase from 12K to 87K. Several solutions to this problem are available, although each solution does have limitations. These are the solutions proposed by this task:

1. Narrow the system bandwidth, and increase near-field probe gain over 10 dB by replacing the waveguide probe with a standard gain horn. Although this solution increases the dynamic range, it also increases the collection time and reduces the accuracy of wide angle data (greater than 10°).

2. Increase power to the mixer with a solid state millimeter amplifier in the measurement receive circuit.

3. Obtain a full band 10 watt TWT and a 60 GHz fundamental frequency synthesizer to maximize transmitted signal to noise ratio.

The hardware estimate in the table below, shows the cost of applicable components to implement all three methods.

Table 7: Hardware Cost Estimate at 60 GHz

Option 1 (26.5 to 60 GHz)

Component	Quantity	Cost(K)
Waveguide Plumbing	na	6
Q-Band Transitions	2	1
Source Frequency Tripler[1,2]	1	3
Harmonic Mixers	8	34
Calibration Hardware	na	12
GASFET Amplifier[2]	8	100
TWT Amplifier[3]	1	137
60 GHz Synthesizer[3]	1	40
Hardware Total[1]	na	56
Hardware Total[2]	na	156
Hardware Total[3]	na	233

Option 2 (U-Band, 40 to 60 GHz)

Component	Quantity	Cost(K)
Waveguide Plumbing	na	3
Source Frequency Tripler[1,2]	1	3
Harmonic Mixers	6	18
Calibration Hardware	na	10
GASFET Amplifier[2]	4	60
TWT Amplifier[3]	1	87
60 GHz Synthesizer[3]	1	40
Hardware Total[1]	na	34
Hardware Total[2]	na	94
Hardware Total[3]	na	161

Option 3 (Single Frequency)

Component	Quantity	Cost(K)
Waveguide Plumbing	na	3
Source Frequency Tripler[1,2]	1	3
Harmonic Mixers	6	18
Calibration Hardware	na	10
GASFET Amplifier[2]	4	33
TWT Amplifier[3]	1	30
Phase Locked Source[3]	1	30
Hardware Total[1]	na	34
Hardware Total[2]	na	67
Hardware Total[3]	na	94

[1]24 dB dynamic range increase by narrowing bandwidth and probing with gain horns
[2]40 dB dynamic range increase with GASFET amplifier, includes 24 dB increase of (1)
[3]80 dB dynamic range increase with TWT and synthesizer, includes 24 dB increase of (1)

Following the acquisition of one of the sets of hardware described above, a performance evaluation will determine the measurement quality possible with the NFML scanner configured to test at 60 GHz. The following table a preliminary estimate of the software upgrades and system testing required for an error analysis of the 26.5 to 60 GHz band.

Table 8: Scanner Calibration at 60 GHz

Task	Hours
Position error correcting software	320
Probe mounting and system calibration	480
Mounting of large aperture antenna	80
Microwave measurements	320
Error Analysis	320
Documentation and Report	160
Labor Total	1680

6.3 Upgrade to 200 GHz

We know of no near-field scanners functioning above 60 GHz, therefore we recommend establishing an experience base below 60 GHz before experimenting above 60 GHz. Upgrading the facility above 60 GHz results in different hardware acquisition problems than the lower frequency applications. Below 60 GHz, although active waveguide band or broader band components are expensive, they are commercially available. Above 60 GHz, however, only the passive components,frequency multipliers, and mixers are available in full waveguide bandwidths. Several techniques exist to bypass this obstacle. One technique is to increase the probe gain, possibly by 20 dB or more over the open-ended waveguide, thus increasing the system dynamic range but reducing the region of reliable pattern data to approximately ±10° of electrical boresight of the probe. For large aperture antennas this limit would not affect data in the normal region of interest. Another technique that can yield increased dynamic range is increasing the maximum LO frequency, thus reducing the harmonic mixing number and its corresponding conversion loss by up to 20 dB. Beyond these modifications received signal power can only be increased by using active amplification devices. These devices typically have bandwidths of less than 5% and also are not production items, purchase of such a device would require prior knowledge of the measurement frequency. Therefore, options 1 and 2 are not available for measurement of large aperture (directivity exceeding 70 dB) millimeter antennas due to the antenna insertion loss. The table below lists the expected hardware costs to implement each of the options described in section 6.1 to 200 GHz.

Not included in the 200 GHz system estimate are some hardware modifications that may be required to the positioning error system, because of the decreasing wavelength. Among these modifications maybe a three-axis positioner with microinch resolution, a laser straightness system, a fiber optic link to the local oscillator, and an autoleveling mount for the test antenna. The need for these systems will be determined by the results of efforts under this and future tasks. An important parameter needing defined by future tasks is whether compensating for positioning error mathematically can be accomplished with sufficient accuracy, or mechanical compensation must be used if the wavelength approaches the magnitude of positioning error. Present data shows the system positioning error having a peak to peak value of 0.06 inches, approximately equal to the wavelength of a 200 GHz signal. In this condition position errors are no longer small relative to wavelength and therefore a two term Taylor series may not be sufficient to correct the positioning errors. The fiber optic link may be needed based on the results of measurements performed under this task. The sources of system drift and cable flexure during a collection were isolated by these measurements and a fiber optic link may reduce these terms.

Table 9: Cost Estimate for Millimeter Wave Measurement System

Option 1: Complete Frequency Coverage

Component	Quantity	Cost(K)
Synthesized Signal Source(from 26 to 110 GHz)	na	300
Frequency Doublers*	2	16
Couplers**	12	14
Horn Antennas**	24	12
Waveguide Plumbing	na	24
Millimeter Absorber Material	100	5
Harmonic Mixers	36	130
Waveguide Vane Attenuators	6	17
Waveguide Sliding Loads and Shorts	12	6
26 to 200 GHz Millimeter Wave System Total	na	519

Option 2: Complete Waveguide Band Coverage (G-Band)

Component	Quantity	Cost(K)
Frequency Multiplier (Output Power < -15 dBm)	1	9
Couplers	2	3
Horn Antennas	4	3
Waveguide Plumbing	na	6
Millimeter Absorber Material	40	2
Harmonic Mixers	6	28
Waveguide Vane Attenuator	1	4
Waveguide Sliding Load and Short	2	1
Single Module Synthesizer (75 to 110 GHz)	1	90
Estimated Costs for a 140 to 220 GHz System	na	142

Option 3: Single Frequency Coverage

Component	Quantity	Cost(K)
Couplers	2	3
Horn Antennas	4	3
Waveguide Plumbing	na	6
Millimeter Absorber Material	40	2
Harmonic Mixers	6	28
Waveguide Vane Attenuator	1	4
Waveguide Sliding Load and Short	2	1
Phase-Locked Single Frequency Source***	1	40
Estimated Costs for a 200 GHz System	na	87

*To cover waveguide bands above 110 GHz, typically 20 dB conversion loss
**Six waveguide bands as listed below

Band	Frequency	Wavelength	
		inches	millimeters
Ka	26.5 to 40.0 GHz	0.295 to 0.445	7.50 to11.32
U	40.0 to 60.0 GHz	0.197 to 0.295	5.00 to 7.50
V	50.0 to 75.0 GHz	0.157 to 0.236	4.00 to 6.00
W	75.0 to110.0 GHz	0.107 to 0.157	2.73 to 4.00
D	110.0 to170.0 GHz	0.069 to 0.107	1.76 to 2.73
G	140.0 to220.0 GHz	0.053 to 0.084	1.36 to 2.14

***Increases dynamic range of system by 30 dB or more

Labor costs to implement and evaluate this system should be approximately equal to the cost estimated for the 60 GHz evaluation and are listed in the table below.

Table 10: Scanner Calibration at 200 GHz

Task	Hours
Position error correcting software	400
Probe mounting and system calibration	560
Mounting of large aperture antenna	160
Microwave measurements	320
Error Analysis	400
Documentation and Report	160
Labor Total	2000

6.4 Estimate Summary

The table below summarizes the estimated initial system costs for the various options discussed in the preceding text. System cost increases are linear for most components with frequency, but increase exponentially system power requirements. Each option listed is self-supporting, for example, the 200 GHz single frequency option will deliver a system fully configured to operate at 200 GHz, however system performance maybe limited by unknown parameters.

Table 11: Millimeter Wave Measurement Upgrade Options

Task	Parts(K)	Labor (Hours)
K-Band System		
18 to 26.5 GHz	10	1200
Minimal Configuration		
26.5 to 60 GHz, Single Frequency	34	1680
40 to 60 GHz, Single Band	34	1680
26.5 to 60 GHz, Full Band	56	1680
Solid State Amplifiers (GASFET)		
26.5 to 60 GHz, Single Frequency	67	1680
40 to 60 GHz, Single Band	94	1680
26.5 to 60 GHz, Full Band	156	1680
Fundamental Synthesized Source and TWTA		
26.5 to 60 GHz, Single Frequency	94	1680
40 to 60 GHz, Single Band	161	1680
26.5 to 60 GHz, Full Band	233	1680
200 GHz Systems		
200 GHz, Single Frequency	87	2000
140 to 220 GHz, Single Band	142	2000
26.5 to 200 GHz, Full Band	519	2000

7.0 Summary and Conclusions

Having completed the work on this task, we will summarize the results and their application to millimeter measurements at the NFML. First, a mathematical model of the predicted system performance showed that the existing facility maybe able to achieve acceptable measurements up to 200 GHz. Second, a series of experiments demonstrated that the model agrees with observed system performance at 18 GHz. Third, based on the measurements and model, a series of far-field parameter accuracies was developed showing acceptable system performance through 200 GHz. Important to this conclusion will be the system dynamic range in final configuration. Fourth, the near-field diagnostic capabilities will allow a rapid optimization of the performance of any antenna within the accuracy of the measurement. Fifth, if the same dynamic range is maintained as the test frequency increases, the instrumentation costs tend to increase geometrically relative to frequency. Commercially available components exist to allow facility coverage to 200 GHz .

Several important issues arose from the work done on this task. The following lists covers the critical issues.

1. Directly correlating microwave and laser straightness data
2. Achieving acceptable system dynamic range at a specific frequency
3. Maintaining system drift low enough to be correctable with current cabling
4. Improving system stability during flexure, possibly by using fiber optics
5. Accurately compensating for scanner position errors
6. Using of LNAs or TWTs to reduce system noise
7. Method of implementing millimeter near-field capability

However, results in this task suggest that these issues are solvable. The best approach should investigate the hardware to verify the performance capabilities predicted by this task. The first phase of this investigation will be the next task measuring system performance up to 26 GHz.

Our recommendation based on past experience and the results of this task is to use an evolutionary approach to increase the maximum system frequency to that desired by the customer. This approach, although appearing initially more expensive, shall result in a thoroughly trained staff prepared to calibrate and measure the final test article to the level that meet or exceed program requirements.

Bibliography

[1]Swokowski, Earl W.: Calculus with Analytical Geometry, Prindle, Weber & Schmidt, Inc., Boston MA, 1975.

[2]Harrington, Roger F.: Time Harmonic Electromagnetic Fields, McGraw-Hill Company, New York NY, 1961.

[3]DuPont: "Teflon, Fluorocarbon Resin", E-05561-3, DuPont, Wilmington NJ.

[4]Bergman, L.A., et al.: "Temperature Dependence for a Single-Mode Fiber", JPL, Pasadena CA, 1981.

[5]Hall, Martin P.M.: Effects of the Troposphere on Radio Communication, IEE, London, England, 1979.

[6]Newell, Allen: "Upper Bound Errors in Far-Field Antenna Parameters Determined from Planar Near-Field Measurements, Part 2: Analysis and Computer Simulation", Lecture Notes for National Bureau of Standards Short Course, Boulder CO, July 1975.

NASA
National Aeronautics and Space Administration

Report Documentation Page

1. Report No.	2. Government Accession No.	3. Recipient's Catalog No.
NASA CR-182014		

4. Title and Subtitle	5. Report Date
Millimeter Wave Near-Field Study	April 1990
	6. Performing Organization Code

7. Author(s)	8. Performing Organization Report No.
Neill Kefauver	MCR-89-575
	10. Work Unit No. 506-44-21-03

9. Performing Organization Name and Address	11. Contract or Grant No.
Martin Marietta Corporation, Astronautics Group Space Systems Company P.O. Box 179 Denver, CO 80201	NAS1-18455
	13. Type of Report and Period Covered Contractor Report

12. Sponsoring Agency Name and Address	14. Sponsoring Agency Code
National Aeronautics and Space Administration Langley Research Center Hampton, VA 23665-5225	

15. Supplementary Notes

Martin Marietta Program Manager: Jim Osborn
Langley Technical Monitor: L. C. Schroeder
Final Report, Task 3

16. Abstract

This report evaluates the possibility of current technology measuring large aperture millimeter wave antennas. Included in this evaluation are a mathematical modeling of system errors, experimental data supporting error model, predictions of system accuracy at millimeter wavelengths, advantage of near-field measurements, and a cost estimate for a facility upgrade. The report emphasizes the use of software compensation and other inexpensive alternatives to develop a near optimum solution to near-field measurement problems at millimeter wavelengths.

17. Key Words (Suggested by Author(s))	18. Distribution Statement
Millimeter Wave, Near-Field, Antenna, Measurement, Fourier Analysis	Unclassified - Unlimited Subject Category 14

19. Security Classif. (of this report)	20. Security Classif. (of this page)	21. No. of pages	22. Price
Unclassified	Unclassified	50	A03